Transient 3D simulation of ^{18}O concentration by codes MODFLOW-2005 and MT3DMS in a regional-scale aquifer system: an example from the Estonian Artesian Basin

Leo Vallner[a], Jüri Ivask[b], Andres Marandi[a], Rein Vaikmäe[b], Valle Raidla[a] and Anto Raukas[c]

[a] Geological Survey of Estonia, Kreutzwaldi 5, 44314 Rakvere, Estonia; leo.vallner@taltech.ee, andres.marandi@egt.ee, valle.raidla@egt.ee
[b] Department of Geology, School of Science, Tallinn University of Technology, Ehitajate tee 5, 19086 Tallinn, Estonia; rein.vaikmae@taltech.ee, juri.ivask@taltech.ee
[c] Institute of Ecology, Tallinn University, Uus-Sadama 5, 10120 Tallinn, Estonia; anto.raukas@mail.ee

Received 26 February 2020, accepted 13 July 2020, available online 18 August 2020

Abstract. It is proved that a transient 3D distribution of ^{18}O concentration in a regional-scale heterogeneous multi-layered aquifer system can be numerically simulated by codes MODFLOW-2005 and MT3DMS as a boundary problem. An optimum method of the transition of the observed negative $\delta^{18}O$ values to respective positive units of the absolute ^{18}O concentration needed for simulations has been substantiated. The practical applicability of the elaborated method has been verified by the reconstruction and interpretation of the geohydrological history of the Estonian Artesian Basin during the Late Pleistocene and Holocene. The adequacy of regional hydrodynamic calculations proceeded by eight consecutive modelling scenarios has been verified by a good correlation between the measured and simulated ^{18}O values. The set of functionally interconnected groundwater flow and ^{18}O transport models forms an integral hydrogeological model of the Estonian Artesian Basin for the last 22 ka. The paper contributes to a wider application of ^{18}O concentration as a conservative tracer in the investigation of the complex problem of groundwater flow and transport in real-world conditions.

Key words: ^{18}O data, solute transport, numerical modelling, environmental tracers, palaeohydrology, Estonian Artesian Basin.

INTRODUCTION

In investigating natural water environments, ^{18}O data have been applied widely: to elucidate the genesis and evolution of waters, to identify the flow components of groundwater systems and to determine physical parameters of flow dynamics (Clark & Fritz 1997; McIntosh et al. 2012; Stotler et al. 2012; Zhao et al. 2018; Kumar et al. 2019). The ^{18}O data are used to establish groundwater recharge history and the aquifer's isolation degree, which are essential for sustainable exploitation and protection of groundwater resources (Person et al. 2012a; Gonçalvès et al. 2015; Beal et al. 2019; Li et al. 2019).

Thereat, $\delta^{18}O$ values are mostly considered as individual records determined for separate sampling points. Their spatial distribution is often calculated by geometric interpolation or even extrapolation for groundwater systems (Wassenaar et al. 2009; Kern et al. 2014; Raidla et al. 2016). This complicates using the ^{18}O content as a tracer in groundwater studies and could cause misinterpretation of the real function of time-dependent hydrodynamic and hydrochemical factors at the formation of the groundwater flow and transport. To a quantitative analysis of these problems, the distribution of the ^{18}O content in a groundwater system should be described by a continuous function $C(x, y, z, t)$, where x, y and z are Cartesian space coordinates, and t is time.

Bowman & Willett (1991) used the solutions of the differential equation describing the 1D convective-dispersive solute transport in a saturated porous environment (van Genuchten & Alves 1982) to study the oxygen isotope exchange between fluid and rock. Person et al. (2012b) modelled the time-dependent distribution of the $\delta^{18}O$ value along with a 1D vertical profile using the same approach. DeFoor et al. (2011) completed 2D models of $\delta^{18}O$ distribution for cross sections on the continental scale to interpret the ice sheet-derived submarine groundwater discharge on Greenland's shelf. Bense & Person (2008)

constructed a heuristic cross-sectional 2D model for an idealized sedimentary basin having a depth of 5 km and length of 700 km, whereby the transient spreading of $\delta^{18}O$ values was calculated for dependence on mechanical ice sheet loading. Beaudoin et al. (2006) simulated the 3D distribution of $\delta^{18}O$ in a quartz tourmaline–carbonate vein field on a rectangular area covering 670 km^2 in Canada. Therrien et al. (2012) created a 3D numerical model *HydroGeoSphere* to describe the subsurface and surface flow and solute transport. Jiang et al. (2019) created a vertical slab model with sizes of 2500 m × 3000 m × 20 m to simulate the 2D fluid–heat–isotope transport by the code TOUGH2 in the Guide Basin, China.

Regardless of the above $\delta^{18}O$ simulation achievements, the authors of this study are not aware of any 3D time-dependent $\delta^{18}O$ models encompassing a real-world multi-layered regional-scale groundwater system with an exhausting profoundness. Such models would be much more trustful information sources for interpreting the environmental problems than solely 2D sections of water-bearing formations.

The main aim of this study is to substantiate theoretically and demonstrate in practice how feasible it is to simulate the time-dependent 3D distribution of ^{18}O in real-world regional-scale heterogeneous aquifer systems to clarify and verify the results of hydrodynamic calculations. The Estonian Artesian Basin (EAB), hydrogeologically profoundly investigated and properly studied for the isotope content of waters, has been depicted as an example of the practical application of the proposed simulation method. In this connection, the additional specific goals of the paper are as follows: (1) to complete a series of mutually linked groundwater flow and ^{18}O transport models based on geological evidences found in the EAB from the period of last 22 ka before present (BP) and (2) to reconstruct by modelling the synchronous hydrogeological situation and to assess its adequacy by the discrepancy between simulated ^{18}O concentrations and the measured ^{18}O values.

ACCOMMODATION OF $\delta^{18}O$ RECORDS TO TRANSPORT SIMULATIONS

The absolute concentration of ^{18}O

The ^{18}O content is conventionally reported in units of parts per thousand (denoted as $\delta^{18}O$, ‰ or per mil) calculated by Eq. (1) (McKinney et al. 1950):

$$\delta^{18}O \text{ (in ‰)} = 1000[(^{18}O_x/^{16}O_x)/(0.0020052 - 1)], \quad (1)$$

where $^{18}O_x/^{16}O_x$ is the ratio of the heavy to light isotope in the sample and the value 0.0020052 in the denominator is the same for the international VSMOW standard (Coplen et al. 2002; IAEA 2017).

The transient 3D distribution of the ^{18}O content in a system of heterogeneous water-bearing layers can be simulated by code MODFLOW-2005 supporting the MT3DMS package which enables the modelling of complex solute transport (Zheng & Wang 1998, 1999; Zheng & Bennet 2002; Harbaugh 2005; Bear & Cheng 2010; Zheng 2010). Thereat, it is necessary to consider the groundwater as a solution in which $H_2{}^{18}O$ molecules represent a solute dissolved in a solvent composed of $H_2{}^{16}O$ molecules. In that case, the motion of $H_2{}^{18}O$ molecules and their mixing with $H_2{}^{16}O$ molecules in the solution (groundwater) saturating the porous medium can be studied as processes of advection, dispersion and molecular diffusion (Crank 1975; Grathwohl 1998).

The MT3DMS package does not accept negative values of the given initial and boundary conditions, except a sole case to eliminate undesired outputs in a multispecies simulation (Zheng & Wang 1998, pp. 6–34). Despite that, the negative $\delta^{18}O$ values, common at isotope investigations, can be made applicable to MT3DMS calculations.

For that purpose, Eq. (1) should be rewritten as

$$^{18}O_x = {}^{16}O_x[(0.0020052 \times \delta^{18}O)/(1000 + 0.0020052)]. \quad (2)$$

Assuming that there is 1 mole of water, the deuterium/protium ratio is not taken into account, ^{17}O abundance is ignored, hydrogen's molar mass is equalized to 1.00794 g/mol and proceeding from Eq. (2), it is possible to calculate the mass concentration of ^{18}O (denoted C_{18O}) in a sample. After reductions and assuming that g/kg ≈ 1000 mg/L, the mass concentration of ^{18}O derived from the value of $\delta^{18}O$ can be calculated as follows:

$$C_{18O} \text{ (in mg/L)} = 2003.499 + 2.004 \times \delta^{18}O. \quad (3)$$

Values of mass concentration C_{18O} calculated by Eq. (3) are used to express the initial and boundary conditions of the MT3DMS simulation models in this study.

Whilst ^{18}O concentration units in mg/L are probably unusual to most researchers, who are accustomed to the $\delta^{18}O$ notation, the latter can be restored from the simulated C_{18O} values by the equation

$$\delta^{18}O \text{ (in ‰)} = (C_{18O} - 2003.499)/2.004. \quad (4)$$

In the following text and figures, $\delta^{18}O$ values are mostly given as ^{18}O simulation results. Adjacently, the respective values of the absolute concentration of ^{18}O are reported in mg/L.

The relationship between long-term mean $\delta^{18}O$ records and their respective C_{18O} characteristics derived by Eq. (3) for the main genetic types of natural waters are given in Table 1. The sampling height of meteoric water was mostly 50–150 m a.s.l. but the sampling interval of basinal brine and glacial meltwater was 100–300 m b.s.l.

Table 1. Characteristics of ^{18}O concentration in natural waters

Water type	$\delta^{18}O$ (‰)	C_{18O} (mg/L)
Dead Sea water (Sofer & Gat 1972)	+6.6	2017
Red Sea water (Sofer & Gat 1972)	+1.3	2006
VSMOW (Clark & Fritz 1997; Stotler et al. 2012)	0	2004
Basinal brine, EAB (Mokrik 2003; Gerber et al. 2017)	–6	1992
Meteoric water, EAB, modernity (Punning et al. 1987; Kortelainen 2007)	–10	1983
Meteoric water, EAB, 12.5–11 ka BP (Arppe & Karhu 2010)	–15	1973
Glacial meltwater, EAB (Vaikmäe et al. 2001; Raidla et al. 2009; Pärn et al. 2015)	–23	1957

Computational adequacy of the absolute concentrations of ^{18}O

To test the adequacy of an MT3DMS output based on the absolute concentrations of ^{18}O, a transient distribution of the ^{18}O concentration $C_{18O}(x, t)$ along a one-dimensional hypothetical generic aquifer was simulated in the interval $0 \le x \le L$ using MT3DMS supported by the MODFLOW-2005 code (Harbaugh 2005). Hereby x was the space coordinate, t was time and L was the flow length.

The flow model completed consisted of 1 layer, presented by 1 row, divided into 150 columns. The parameters used in the simulation were as follows: cell width along the row $\Delta x = 2000$ m, cell width along columns $\Delta y = 1000$ m, layer thickness $\Delta z = 1$ m, length of the homogeneous strip aquifer $L = 300$ km, hydraulic conductivity $K_x = 7$ m/day, effective porosity $\Theta = 0.15$, dispersion coefficient $D_L = 10$ m^2/day and specific storage $S_s = 10^{-5}$ 1/m. In the flow model, the first and last columns were constant-head boundaries providing the uniform hydraulic gradient $I = 0.002$ and pore water average linear velocity $v = I K_x/\Theta = 0.09$ m/day along with the steady-state flow. The length and values of filtration parameters of the strip aquifer are typical for the groundwater transport flowpaths on the EAB.

It was presumed that initially $[C(x, 0)]$ the aquifer was saturated with basinal brine with $\delta^{18}O = –6‰$ (1992 mg/L). The boundary conditions given for the transport model for the time $0 < t \le 10$ ka were as follows: at $C(0, t)$ $\delta^{18}O = –24‰$ (1955 mg/L) and at $C(L, t)$ $\delta^{18}O = –6‰$ (1992 mg/L). According to these conditions, the ^{18}O-depleted glacial meltwater intruded into the aquifer containing basinal brine in section $x = 0$ of the one-dimensional flow at the time $0 < t \le 10$ ka.

Simulations were carried out by MT3DMS v5.3 using the Implicit Generalized Conjugate Gradient solver and the Upstream Finite Difference method at the Courant number of 0.75 (Zheng 2010). The results represented in Fig. 1 show that the area of the imaginary aquifer, where the initial ^{18}O concentration of water was diluted to the ^{18}O concentration of glacial meltwater, advanced to the flow section $x \approx 170$ km during 10 ka. In the remaining portion of the aquifer, the dilution degree of brine by glacial meltwater decreased monotonically. For example, the share of glacial meltwater was about 64% in the flow section $x = 240$ km, and 27% in the section $x = 280$ km at $t = 8$ ka. It means that the mixing of the two genetic types of water in the aquifer was substantially influenced by mechanical dispersion corresponding to the given model parameters (Fetter 1993; Grathwohl 1998; Zuber et al. 2011).

The parameters used in the above MT3DMS solution were put into the 1D analytical solution of the same problem obtained by van Genuchten & Alves (1982) for a range $0 \le x \le \infty$ at boundary conditions $C(0, t) = \text{const}$ and $\partial C(\infty, t)/\partial x = 0$. Generally, the discrepancy between the results of numerical and analytical simulations was less than 1% in the range x studied. This discrepancy could be explained by computational allowances made (quasi-one-dimensionality versus a 'real' one-dimensionality, numerical approximations, etc.).

Thus, the results of the described test simulation are reasonable and in compliance with the fundamentals of the groundwater transport theory (Ogata & Banks 1961; Crank 1975; van Genuchten & Alves 1982; Yates 1992; Fetter 1993; Liedl et al. 2011). It proves that the derived absolute ^{18}O mass concentrations can be used as input data for MT3DMS to simulate the 1D transient distribution of the ^{18}O content in a homogeneous strip aquifer.

STUDY AREA

Hydrogeological setting

The EAB is a part of the homocline formed on the southern slope of the Fennoscandian Shield (Mokrik 2003; Vallner & Porman 2016) encompassing the territory of Estonia (*ca* 45 000 km^2) (Fig. 2) and its closely surrounding areas of the Baltic Sea and the Gulf of Finland (25 000 km^2) (Perens & Vallner 1997). The EAB can also be considered as the northeastern part of the Baltic Artesian Basin (BAB), which embodies the Baltic States, the border areas of Russia, Poland and Belarus and a large portion of the Baltic Sea (Mokrik 2003).

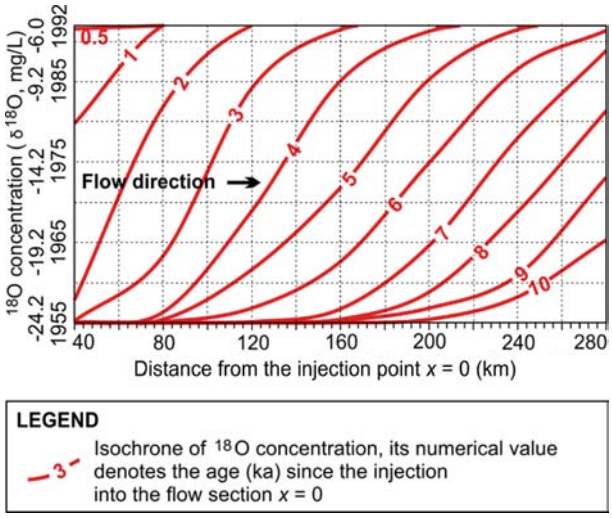

Fig. 1. Development of a quasi-one-dimensional dilution of ^{18}O concentration due to a continuous injection at location $x = 0$, during the time $0 < t \leq 10$ ka.

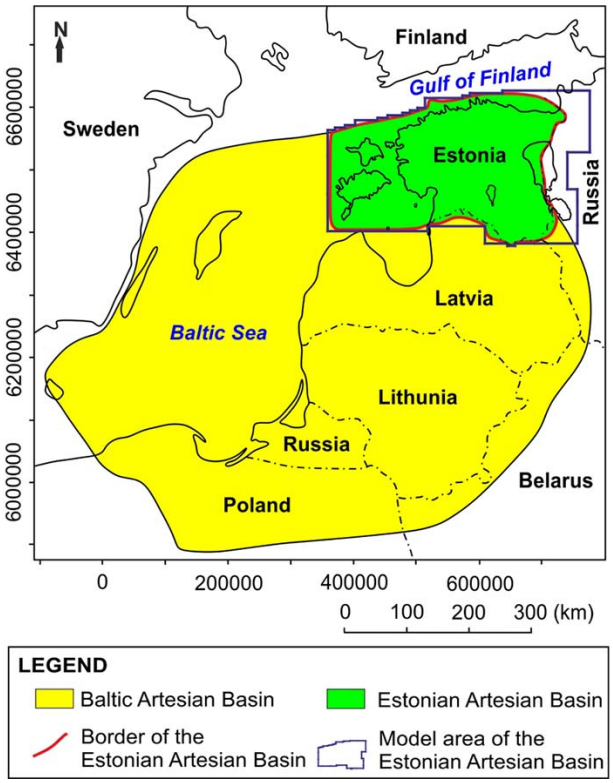

Fig. 2. Location of the study area. The *Estonian Coordinate System of 1997* (GeoRepository 2016) is used here and hereinafter at every figure provided by geographical coordinates given in metres.

The contemporary topography of the EAB is flat or slightly hilly and dissected by deep ancient valleys (Fig. 3). The average absolute height is about 50 m; only a few areas in its southeastern part are 250–300 m above the sea level. The Baltic Sea with the Gulf of Finland is the main drainage basin, Lake Peipsi with an elevation of 30 m above sea level is the second largest. Quaternary deposits (Q) with the usual thickness of 3–30 m, but occasionally over 100–150 m (Fig. 4), consisting predominantly of till and glaciolacustrine and glaciofluvial sandy and loamy deposits form the uppermost aquifer system (Perens & Vallner 1997). In the southern and restrictedly in the eastern parts of the study area, Quaternary deposits cover the terrigenous Devonian aquifer system (D), which is divided into the upper (D_2) and lower ($D_{2\text{-}1}$) aquifers separated by the regional D_2Nr aquitard. In North and Central Estonia, Quaternary deposits lie on the outcrop of the Silurian–Ordovician aquifer system (S–O) consisting of limestones and dolostones. Their lower part forms the regional S–O_r aquitard.

Below come the Ordovician–Cambrian (O–Cm) and Cambrian–Vendian (Cm–V) aquifer systems consisting mostly of sandstone with clay and siltstone interbeds. The Lükati–Lontova aquitard (Cm_1Lk–Ln) separates the two systems. The Cambrian–Vendian aquifer system (CVAS) including the upper Voronka (V_2Vr) and the lower Gdov (V_2Gd) aquifer, with the Kotlin aquitard (V_2Kt) between them

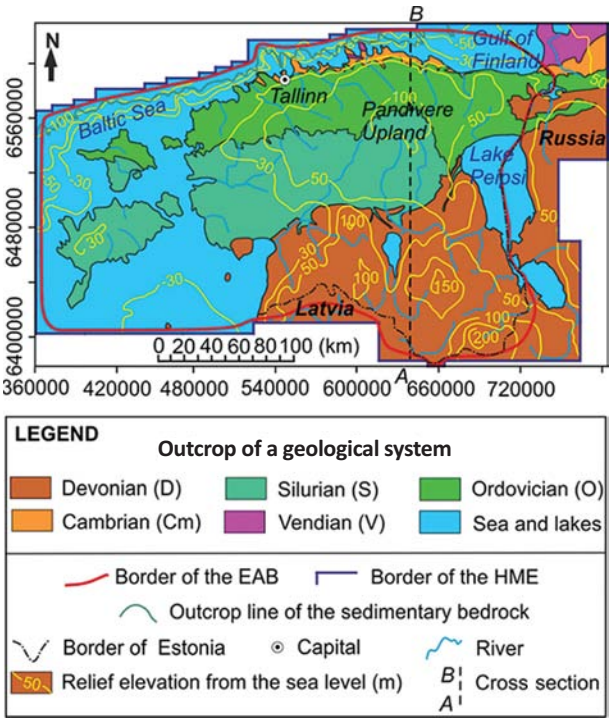

Fig. 3. The Estonian Artesian Basin (EAB) and the Hydrogeological Model of Estonia (HME).

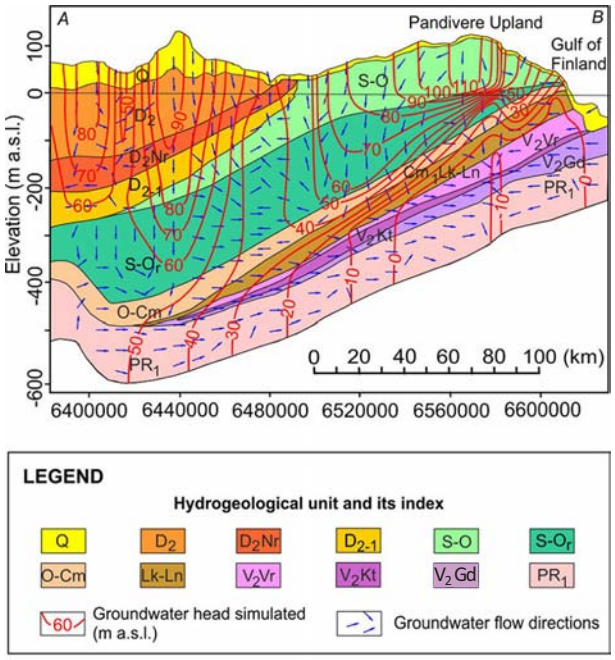

Fig. 4. Hydrogeological units and distribution of the groundwater hydraulic head simulated in the EAB cross section *A–B* in 1976 (see Fig. 3 for cross section location).

in the eastern part of the study area, crops out along the northern coast of Estonia on the bottom of the Gulf of Finland. The CVAS pinches out in the southwestern area of the EAB, where the O–Cm aquifer system represents the lowermost terrigenous water-bearing beds. The depth of the crystalline Proterozoic basement (PR_1) from the ground surface increases from 100–150 m on the coast of the Gulf of Finland to 500–800 m along the southern border of the EAB.

The lateral hydraulic conductivity of sandstones, limestones, dolostones and sandy Quaternary deposits is usually between 2 and 8 m/day, the storage coefficient ranges mostly from 10^{-5} to 10^{-3} 1/m (Perens & Vallner 1997; Vallner & Porman 2016). The lateral hydraulic conductivity of karstified carbonate rocks can reach 50 m/day, or even more. The vertical hydraulic conductivity of aquitards mostly varies in an interval of 10^{-9}–10^{-2} m/day.

The strata lying at less than 200–300 m below sea level usually contain fresh water. However, in deeper ones, the Na–Cl type of groundwater occurs, whose total dissolved solids value increases southwards up to 22 g/L.

The bedrock is cut by quite a dense network of pre-Quaternary valleys, whose bottoms lie at up to 130 m below the present sea level. The ancient buried valleys are mostly filled by different loose Quaternary deposits.

During the last seven decades, intensive groundwater abstraction for water supply and mine dewatering has taken place in the model area. The pumping activity culminated around 1990. The mean yearly value of groundwater abstraction between 1950 and 1990 was recorded in 1976. Because of groundwater withdrawal basin-wide head depressions formed in several aquifers (Fig. 4), engendering the intrusion of unpotable water towards groundwater intakes (Gavrilova et al. 2010; Marandi & Vallner 2010; Vallner & Porman 2016). This phenomenon is described in more detail hereinafter in the subsection 'The period of intensive groundwater development (Model 8)'.

Scandinavian ice sheets repeatedly covered the EAB in the Pleistocene. The existence of the Elsterian, Saalian and Weichselian glaciations and the Holsteinian and Eemian interglaciations has been determined in Estonia (Raukas 1986; Elverhøi et al. 1993; Siegert 2001; Lambeck et al. 2009; Kalm et al. 2011; Lasberg & Kalm 2013). Recharge of aquifers with glacial meltwater occurred during both glaciation and deglaciation phases (Vaikmäe et al. 2001, 2008). The EAB became free from the last, Weichselian glaciation at about 12 ka before present (BP) (Kalm et al. 2011).

Isotope data

In Estonia, research of environmental isotopes in the hydrosphere was initiated in the 1980s and systematically developed up to this day (Punning et al. 1987; Vaikmäe & Vallner 1990; Vaikmäe et al. 2001, 2008; Raidla et al. 2009, 2012, 2019; Marandi & Vallner 2010; Pärn et al. 2015, 2016, 2019; Koit et al. 2020). The ^{18}O sampling data used in the current study were taken from the *Baltic groundwater isotope-geochemistry database* (Vaikmäe et al. 2020). This database contains isotopic, chemical and noble gas composition data of 1081 groundwater samples collected in Estonia, Latvia and Lithuania during the period of 1974–2017. The isotopic composition of modern precipitation from the Vilsandi and Tartu stations of the Global Network of Isotopes in Precipitation (GNIP) in Estonia from 2013 up to 2018 are available via the GNIP network (IAEA/WMO 2018).

All the main hydrogeological units of the EAB mentioned above have been sampled. However, deep layers have been much more explicitly sampled in the northern part, because in South Estonia, deep boreholes opening the lowermost water-bearing layers at depths of 400–700 m are relatively rare.

Prior to 2010, the stable isotope ratios of oxygen were measured with a Finnigan MAT Delta-E mass spectrometer using the conventional CO_2 equilibration technique. The reproducibility of measurements was ±0.1‰ for $\delta^{18}O$. For samples collected since 2010, the isotope ratios of both hydrogen and oxygen were measured with cavity ring-down laser spectroscopy (CRDS) using a Picarro L2120-i Isotopic Water Analyzer. The reproducibility of measurements was ±0.1‰ for $\delta^{18}O$ and ±1‰ for δD.

The ^{18}O data of 199 most representable sampling wells from the mentioned database covering the entire EAB (Vaikmäe et al. 2020) were selected for the current study (Fig. 5; also supplementary data in the Appendix at https://doi.org/10.15152/GEO.501).

Regional groundwater flow and transport models

Already in 2002, a regional 3D flow model representing the contemporary hydrogeological situation of the EAB, called the Hydrogeological Model of Estonia (HME), was constructed by using the Visual MODFLOW code (Vallner 2003; Vallner & Porman 2016). Later, the model was significantly elaborated by incorporating supplementary data and upgraded to the latest versions of Visual MODFLOW Classic (VMC) supporting MODFLOW-2005 and MT3DMS (WH 2015). The preliminary steady-state flow model was developed into a coupled density-dependent transient flow and transport model. Currently, the interface VMC of the HME has been duplicated by interface ModelMuse (Winston 2019).

The model involves all the main aquifers, aquifer systems and aquitards in the area of 88 000 km^2 (Figs 3, 4), which are represented by 13 model layers. The study area has been covered with a virtual rectangular grid at a spacing from 1000 to 4000 m for finite-difference

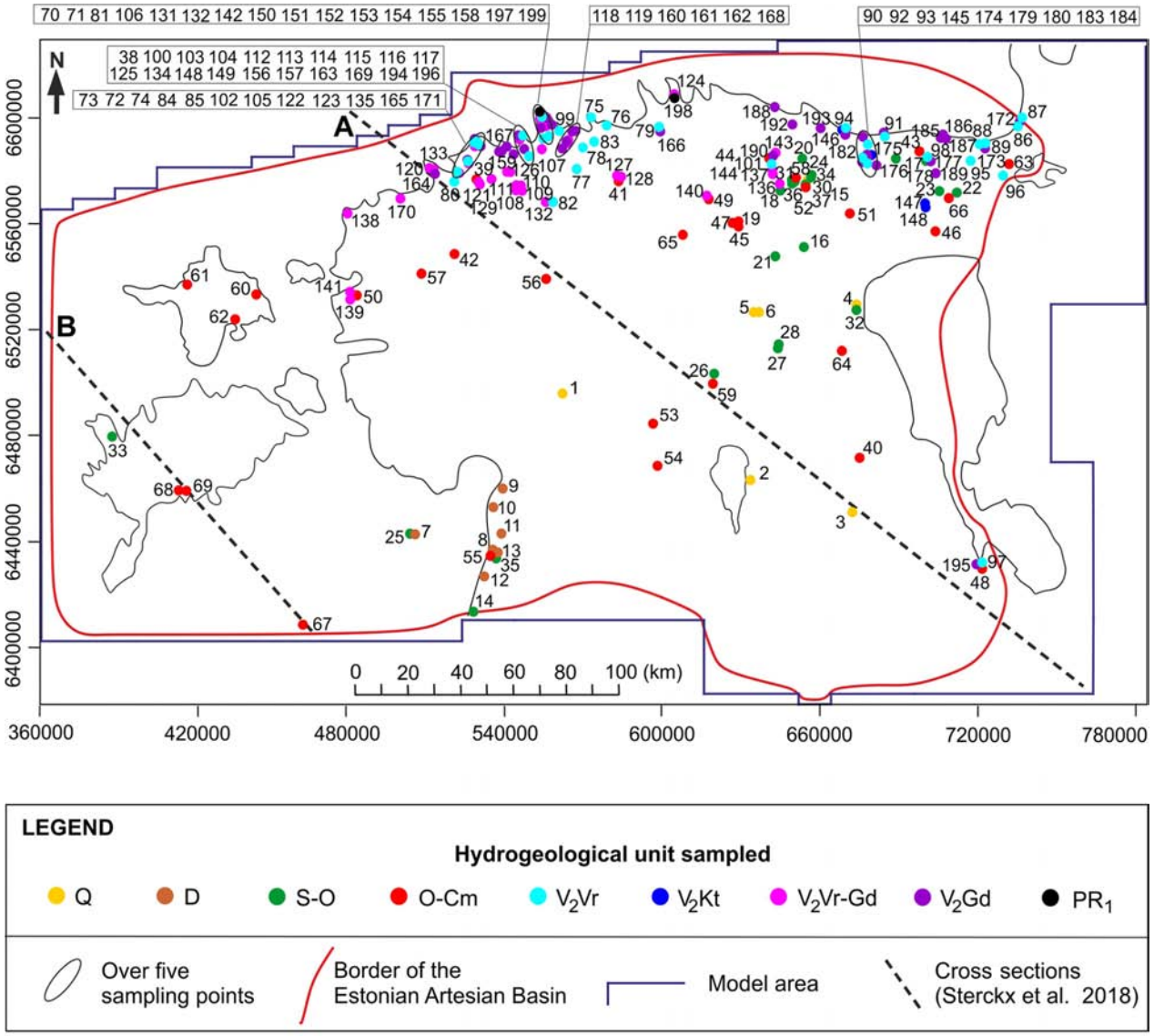

Fig. 5. Sampling points of ^{18}O analyses used for palaeohydrogeological reconstructions (see the Appendix at https://doi.org/10.15152/GEO.501).

discretization. The top boundary of the model coincides with the ground surface or with the bottom of rivers, lakes and the sea. A virtual surface lying at a depth of 100 m beneath the upper surface of the crystalline basement acts as a supposed impermeable bottom boundary of the model. The thickness of the water-bearing formation modelled varies from 100–150 m in the north to 600–900 m along the southern border of the area.

The Dirichlet type of boundary conditions was mostly given to the outer boundaries of the model layers. Groundwater discharge through numerous springs was modelled by the Neumann type of boundary conditions. The Cauchy type of boundary conditions was used to define the relationship between surface water bodies and the groundwater system. The long-term groundwater discharge into the river net was established by more than 100 hydrological river gauging stations during several decades. All groundwater intakes with their abstraction rates were incorporated into the model. The results of about 1000 time-drawdown and distance-drawdown pumping tests were used to characterize the hydraulic conductivity, the specific storage and the effective porosity of aquifers.

The regional model was calibrated against the measured mean elevations of the groundwater heads and rates of the base flow, which were recorded in 1976, 1990, 1998, 2006, 2013 and 2015 (Vallner & Porman 2016). The maximum differences allowed between the measured and modelled hydraulic heads and rates of the base flow were ≤3.5 m and ±20%, respectively. Corrections of hydrogeological parameters introduced by model calibration remained within the acceptable range. The correlation coefficients reaching 0.85–0.95 were obtained between simulated and measured parameters.

The fully calibrated HME has been tested and used for profound investigation of groundwater resources and completing detailed water budgets for Estonia (Gavrilova et al. 2010; Vallner & Porman 2016; Marandi et al. 2019). Problems of the contaminant transport were analysed using the MT3DMS and SEAWAT packages of the model (Marandi & Vallner 2010; Vallner et al. 2015).

The 2D groundwater flow and distribution of $\delta^{18}O$ were simulated for two cross sections of the EAB (Fig. 5) by the numerical model FEFLOW 6.2 from the beginning of the Last Glacial Maximum to the present day (Diersch 2014; Sterckx et al. 2018). Thereat, the input $\delta^{18}O$ data were selected within 20 km across each cross section from various former research reports.

MODELLING CONCEPTION

Fundamentals

The climatic, hydrological and hydrogeological conditions forming the groundwater flow and its isotope characteristics changed drastically due to the last glaciation, deglaciation, evolution of the Baltic Sea and groundwater development in the EAB during the last 22 ka. This period was modelled by eight complementary steady-state 3D groundwater flow models (Table 2). Each of the complementary flow models corresponded to a set of boundary conditions reflecting a certain average of palaeogeographical and geohydrological situations specified according to former investigations (Raukas 1986; Elverhøi et al. 1993; Siegert 2001; Lambeck et al. 2009; Kalm et al. 2011; Lasberg & Kalm 2013; Vallner & Porman 2016; Shackleton et al. 2018; Malov & Tokarev 2019). The time-dependent 3D distribution of ^{18}O concentration as a *conservative tracer* (Clark & Fritz 1997) was also simulated by eight MT3DMS transport models coupled and synchronized with the complementary flow models mentioned.

The initial and boundary conditions were embedded into complementary models as different *constant steady-state values* of the hydraulic head $h(x, y, z)$ and concentration $C_{18O}(x, y, z)$. Eight sequential flow and transport simulations were performed. The distribution of the ^{18}O concentration simulated by the previous model was imported into the next one as its initial condition. This way, all complementary models were functionally connected and, together, they formed an integrated

Table 2. Time spans of complementary hydrogeological models

Model	Time span (ka BP)		Palaeogeographical and hydrogeological situation
	Start	End	
1	22.0	20.0	The ice sheet covering the northwestern part of the EAB
2	20.0	18.0	The ice sheet covering the entire EAB, Last Glacial Maximum
3	18.0	14.7	Thinning of the continental ice cover due to ice melting
4	14.7	12.0	Continental ice sheet gradually retreating from the EAB
5	12.0	10.3	Formation of the Baltic Ice Lake and flooding of West Estonia
6	10.3	5.0	Early evolution stages of the Baltic Sea in the Holocene
7	5.0	0.1	Formation of the contemporary topography
8	0.1	0	Intensive groundwater development in the EAB

transient calculation unit suitable for interpreting the successive geohydrological events.

The flow and transport models completed relied upon the geometry and layers' hydraulic properties of the HME, insofar as its adequacy was verified by former successful practical applications and repeated multi-target calibration tests during the last four decades. The advection term of the differential equation describing the ^{18}O distribution was solved by Implicit Generalized Conjugate Gradient solver using the Upstream Finite Difference method at the Courant number of 0.75 (Zheng 2010). In transport models, the value of the longitudinal dispersivity varied from 10 to 200 m; the ratios of horizontal and vertical dispersivity to the longitudinal one were mostly 0.1 and 0.01, respectively. The diffusion coefficient was generally 1×10^{-4} m^2/day. The effective porosity accepted was 0.2–0.3 for Quaternary deposits, 0.15–0.2 for sandstones and 0.01–0.03 for limestones, dolostones and crystalline rocks. The grid Péclet number ranged from 5.0 until 400 (Huysmans & Dassargues 2005).

The groundwater flow directions, velocities, rates and budget characteristics were simulated for every 3D complementary flow model. The concentration $C_{18O}(x, y, z, t)$, depending importantly on the dynamics of groundwater flows, was simulated by the transport code MT3DMS. Thereat, the main genetic components of water and their blends forming the EAB's ^{18}O concentration budget were distinguished (Fig. 6A–D).

Initial conditions of transport models

The area of the EAB was probably ice-free during the Early Weichselian Glacial Substage between 115 and 68 ka BP (Siegert 2001; Kalm et al. 2011). Periglacial climatic conditions likely also prevailed in the Middle Weichselian when a directly dated ice-free period occurred between 44 and 22 ka BP. Depressions of the Baltic Sea and the Gulf of Finland filled with water existed already, and the mainland of Estonia was above the sea level (Fig. 6A). The maximum relative height of the ground surface at the southeastern boundary of the EAB above the Middle Weichselian sea level was probably 300–400 m. Thus, the general hydrodynamic situation was quite close to the present one and groundwater in the CVAS flowed towards the depressions of the Baltic Sea and the Gulf of Finland under the hydraulic gradient of about 0.0003. In that period, *deep basinal brine* (denoted as B below) from the central part of the BAB had mostly displaced the water of previous glaciations and interglaciations that had intruded into the O–Cm aquifer system and the CVAS in the Early and Middle Pleistocene, or even earlier.

The basinal brine was predominantly formed by the mixing of synsedimentary fluids with meteoric waters during the Pre-Quaternary and its $\delta^{18}O$ value ranged from –2‰ to –10‰ (Mokrik 2003; Gerber et al. 2017). The *initial* $\delta^{18}O$ value of the basinal brine (B) for transient concentration simulations was taken equal to –6‰ (C_{18O} = 1992 mg/L) at 22.0 ka BP in the current study (Tables 2 and 3), because similar $\delta^{18}O$ values mostly ranging from –6‰ to –5‰ were recorded in the Cambrian waters of the BAB at depths over 800 m b.s.l. in Latvia (Babre et al. 2016), at 350–400 m in Gotland (Sweden) and at 1800–2900 m in the Aisčiai region (Lithuania) (Mokrik & Mažeika 2002).

Ancient groundwater (A) formed by the mixing of meteoric water and glacial meltwater before the Late Weichselian glaciation filled the upper part of the EAB overlying the O–Cm aquifer system at 22.0 ka BP. Hereby it is import to point out that this genetic type of groundwater is also called formation water, relict water or even old brines by other researchers (e.g. Raidla et al. 2009; Gerber et al. 2017). In accordance with general scientific postures (Mokrik 2003; Jiráková et al. 2011; Gerber et al. 2017), it was assumed that the $\delta^{18}O$ value of the ancient water ranged from –14‰ to –8‰ (C_{18O} = 1975–1988 mg/L). The *initial* $\delta^{18}O$ value of the ancient water A for transient concentration simulations was taken equal to –14‰ (C_{18O} = 1975 mg/L) at 22.0 ka BP. The hypothetical distribution of ancient groundwater and basinal brine in the EAB described above (Fig. 6A) was set up as the principal initial condition for the whole ^{18}O transport modelling.

Table 3. ^{18}O concentration zones

Genetic type of water	Index	$\delta^{18}O$ limits (‰)	Concentration (mg/L)
Ancient groundwater	A	–14 to –8	1975–1988
Deep basinal brine	B	≥–6	≥ 1992
Glacial meltwater	G	–24 to –18	1955–1967
Modern meteoric water	M	–11.5 to –8	1981–1988
Blend of ancient groundwater and basinal brine	AB	–8 to –6	1988–1992
Blend of ancient groundwater and glacial meltwater	AG	–18 to –14	1967–1981
Blend of basinal brine and glacial meltwater	BG	–18 to –6	1967–1992
Blend of glacial meltwater and modern meteoric water	GM	–18 to –11.5	1967–1981

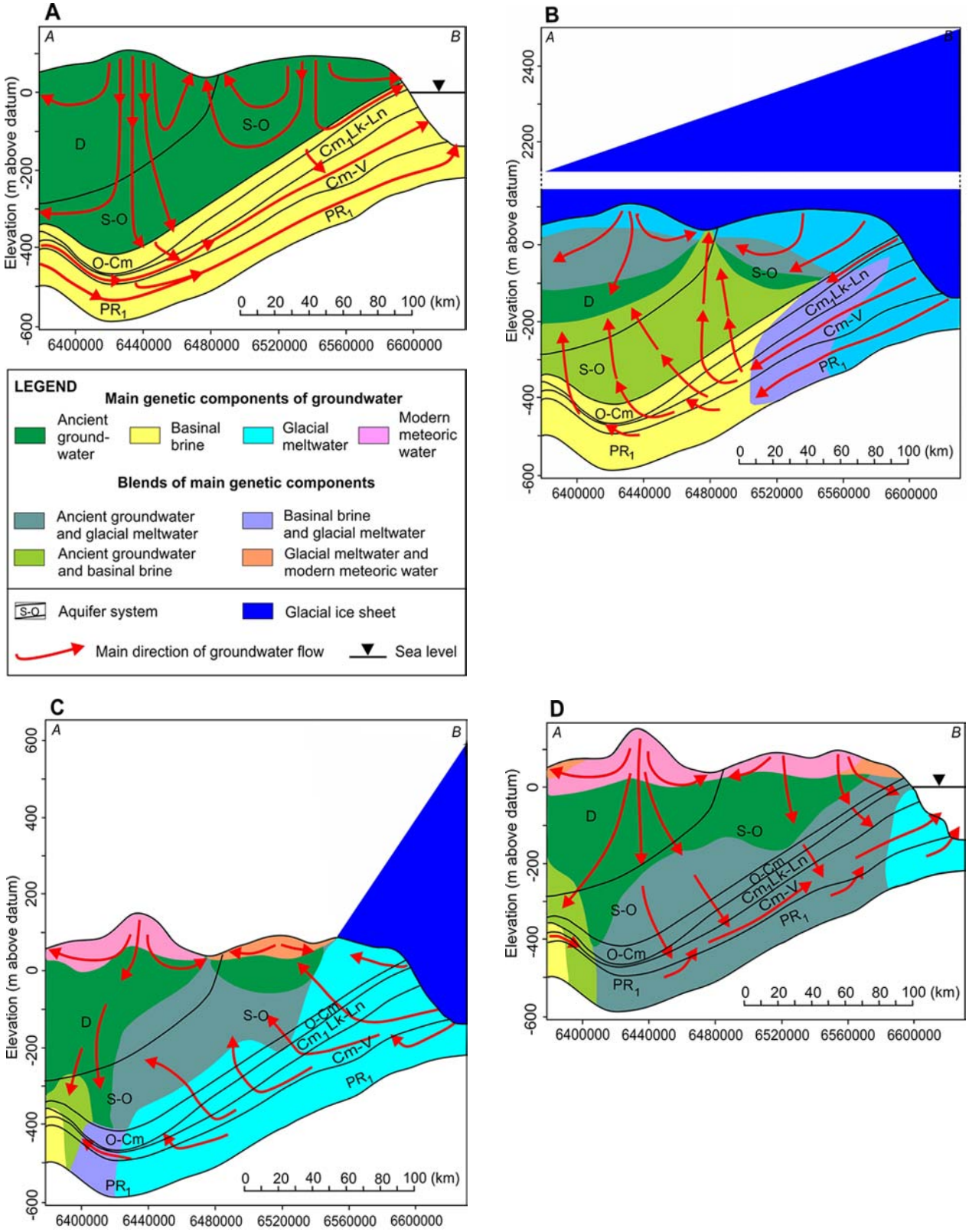

Fig. 6. Conceptual models of main genetic types of water and their blends, and principal directions of the groundwater flow in the EAB at (**A**) 22.0, (**B**) 18.0, (**C**) 12.7 and (**D**) 0.1 ka BP (see Fig. 3 for the cross section location).

Boundary conditions

The outer boundaries of complementary flow models coincided with those of the HME, but the distribution of hydraulic heads along these boundaries was modified by means of the *Constant Head (CHD) Boundary Condition* of the VMC according to stresses caused by the thickness of the ice sheet and vertical movements of the Earth's crust due to isostatic processes. Thereby, it was presumed that the hydraulic head h beneath the ice sheet was proportional to the ice height η (Boulton et al. 1995):

$$h = 0.9\eta. \quad (5)$$

It was supposed that groundwater recharge took place beneath the continental ice sheet covering the EAB partially or completely during the time interval from 22.0 to 12.0 ka BP (Fig. 6B, C). The continental ice melted from the underside due to frictional heating and because of an upward heat transfer in the Earth's crust. A portion of subglacial water also came into being by the melting of top layers of the glacier at its retreat. All subglacial water formed in such way is called *glacial meltwater* (G) and is considered as one of the main genetic components of the EAB water budget in this study (Fig. 6A–D). The glacial meltwater encroached into the uppermost layers transversally, but into deeper ones also via ancient valleys. A great portion of glacial meltwater intruded laterally into deep layers from the depression of the Baltic Sea, due to high pressure generated by the overlying glacier (Fig. 6B; Boulton et al. 1995).

The infiltration of meteoric water into the EAB restored in the Late Pleistocene when the ice sheet perished from the southeast corner of Estonia. In the current paper, the term *modern meteoric water* (M) is used to refer to the groundwater main genetic component emerged from precipitation after this time. The filtration intensity of glacial meltwater and meteoric water into the subsurface was given by the *Recharge Boundary Condition* of VMC. Thereat, the infiltration rate decreased up to ten times in the periglacial area during the interval from 14.7 to 12.0 ka BP compared with present-day infiltration to account for the possible hindering impact of permafrost on groundwater recharge.

For MT3DMS runs it was presumed that the $\delta^{18}O$ values of glacial meltwater and modern meteoric water ranged respectively from –24‰ to –18‰ (C_{18O} = 1955–1967 mg/L) (Olausson 1982; Vaikmäe & Vallner 1990; Vaikmäe et al. 2001, 2008; Raidla et al. 2009, 2012; Jiráková et al. 2011; Pärn et al. 2015; Gerber et al. 2017) and from –11.5‰ to –8‰ (C_{18O} = 1981–1988 mg/L) (Punning et al. 1987; Kortelainen 2007; Raidla et al. 2016). Such ^{18}O concentrations were assigned to infiltration engendered by the *Recharge Concentration Boundary Condition* of MT3DMS into transport models.

It is rational to distinguish the spreading and mixing zones of different genetic components of water formed during ^{18}O mass transport in the EAB (Tables 2, 3; Figs 6A–11). The mixing zones of *ancient groundwater and basinal brine* (AB), *ancient groundwater and glacial water* (AG), *basinal brine and modern meteoric water* (BG) and *glacial water and modern meteoric water* (GM) are mostly delimited by specific values of the simulated ^{18}O content.

To distinguish the borders of water genetic components, the 3D distribution of groundwater heads and corresponding flow vectors of direction, velocity and rate were calculated by VMC packages for complementary Models 1–8. The results of flow modelling depicted by head isolines and arrows showing the flow direction were juxtaposed with ^{18}O concentration data in Figs 7–11. The borders of groundwater genetic zones were estimated by following the changing trend of ^{18}O concentration along the flow directions. Thereat, the automated colour shading of ^{18}O concentration provided by VMC output packages was taken into account (Fig. 7). Partially, the MODPATH code was used to track the transient development of transport flows. The pumping rates of groundwater intakes were embedded into Model 8 as Cauchy boundary conditions through the VMC unit *Pumping Wells* managing the *WEL Package* of MODFLOW-2005.

MODELLING RESULTS

Glaciation (Models 1 and 2)

The ice sheet of the Late Weichselian glaciation moving predominantly to the southeast reached the northwestern part of the EAB at 22 ka BP. Next, the continental ice advanced to the south and southeast, completely covering the EAB (Siegert 2001; Kalm et al. 2011). At the Last Glacial Maximum occurring at 18 ka BP, ice thickness reached about 2700 m in the northwest corner of the EAB and about 2100 m in its southeast corner (Elverhøi et al. 1993) (Fig. 7A). The hydraulic head of groundwater reached up to 2500 m in the northwest corner of the EAB at 18 ka BP. At the same time, the hydraulic head was 1700 m and 1900 m in the southwest and southeast corners of the EAB, respectively. Hereby, it is necessary to stress that the given elevations here and hereinafter have been calculated in relation to the depth of the crystalline basement.

The hydrodynamic simulations performed by Models 1 and 2 (Table 2) showed that during glaciation a complete rearrangement of groundwater flow directions took place because of the changing hydraulic head in the EAB. The infiltration of meteoric water was gradually replaced by

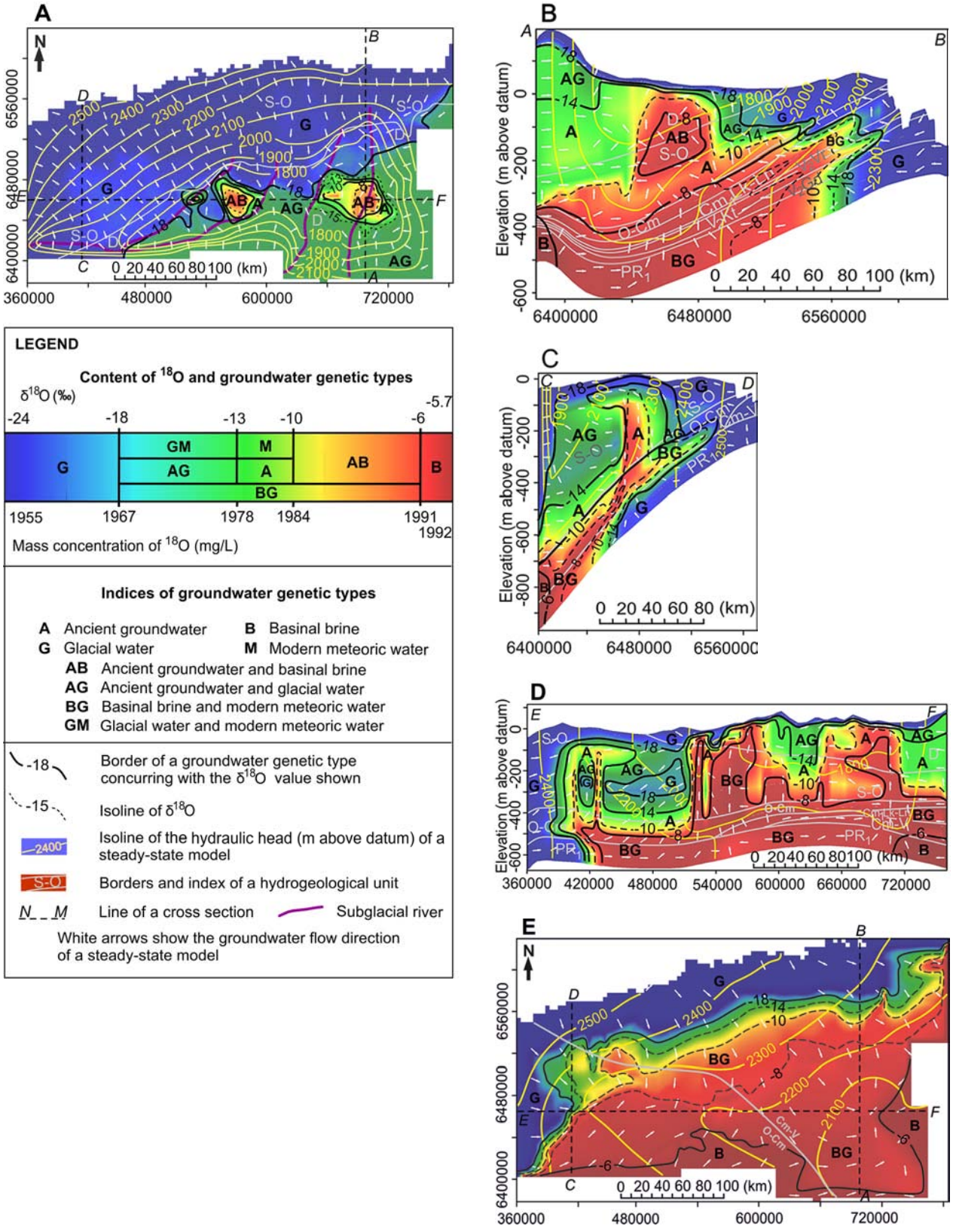

Fig. 7. Groundwater head, flow direction and ^{18}O concentration at 18.0 ka BP (Model 2): (**A**) in the upper layers of the Devonian and Silurian–Ordovician aquifer systems, in cross sections (**B**) *A–B*, (**C**) *C–D*, (**D**) *E–F*, and (**E**) in the Ordovician–Cambrian and Cambrian–Vendian aquifer systems.

the vertical intrusion of glacial meltwater into the subsoil (Fig. 7A, B). On the other hand, the discharge of ancient groundwater and basinal brines from the layers of the EAB in depressions of the Baltic Sea and the Gulf of Finland was displaced by reversed flows, i.e., by the lateral encroachment of glacial water into bedrock layers (Fig. 7B–E). Deep groundwater partially rose upwards and was drained by a network of subglacial currents (Fig. 7A–C).

According to the Mass Balance Report of VMC, the total amount of glacial meltwater encroached into the EAB reached at least about 8200 km^3 during the glaciation period from 22 to 18 ka BP. This corresponds to a subglacial ice melt rate of 0.03 m/year. Such a result corresponds to findings of Lemieux et al. (2008) who have proved that the bulk of the infiltration of the subglacial meltwater into the subsurface can occur even during the growing phase of the ice sheet. In the same time interval, the amount of infiltrated meteoric water was 3200 km^3, the lateral outflow through the borders of the EAB was 400 km^3 and the total discharge of groundwater formed in the channel network beneath the ice sheet and in the area uncovered by continental ice was 11 000 km^3. The mean intensity of the subglacial runoff was about 1.3 L/(sec × km^2), i.e., approximately 90% of the contemporary base flow (Vallner & Porman 2016).

The ^{18}O transport simulation verified and supplemented the results of hydrodynamic modelling. The simulated ^{18}O mass concentrations showed that glacial meltwater intruded downwards from the ground surface even into the upper part of the Silurian–Ordovician regional aquitard forming the clearly identifiable concentration zones G and AG in the northwestern part of the EAB at 18 ka BP (Fig. 7A–D). Since the beginning of glaciation, the outer border of the modelled zone G, where $\delta^{18}O = -18‰$ (C_{18O} = 1967 mg/L), had advanced from the outcrop of the CVAS towards the mainland of the EAB, mostly by 50–70 km during 4 ka, i.e. with the velocity of 12–18 m/year, or 0.03–0.05 m/day (Fig. 7E). The upconing of deep water due to the draining effect of subglacial streams occurred mainly in the southern part of the EAB. The rising basinal brines B intruded into the ancient groundwater A from underneath, forming the mixing zone AB (Fig. 7B, D).

Deglaciation (Models 3 and 4)

At about 18 ka BP, the deglaciation of the BAB began. By 14.7 ka BP, ice thickness had diminished to 100–200 m in the southeast corner of the EAB, but was still about 2200 m in the northwest corner of the EAB (Siegert 2001). Gradually, Estonia became free from the continental ice at the end of the Pleistocene at 13.7 ka BP; most of South Estonia and the Pandivere Upland were ice-free but partly surrounded by local large ice-dammed lakes. The highest elevations of the topography were about 100 m above the level of lakes in the ice-free part of the EAB. However, the ice sheet having the maximum thickness of up to 1800 m covered Northwest Estonia, still generating subglacial meltwater (Fig. 8A).

The subglacial groundwater recharge continued mostly at the rate of 0.02–0.04 m/year during the entire deglaciation period. Due to the diminishing ice-covered area, the amount of glacial meltwater encroaching into the EAB gradually decreased as well and its total amount did not exceed 3000 km^3. At 13.7 ka BP, due to the load of the existing ice sheet in Northwest Estonia, glacial meltwater continued its lateral flux under hydraulic head gradients from 0.002 to 0.005 in the south and southwest directions in the CVAS.

Sequential simulations of ^{18}O mass concentration proceeded by Models 3 and 4 (Table 2) proved the veracity of this hydrodynamic conception based on geological evidence. The modelled contour of $\delta^{18}O = -23‰$ (C_{18O} = 1958 mg/L) coincided with the southern margin of the ice sheet established by geological data marking the area, where glacial meltwater still infiltrated into the subsoil (Fig. 8A). The $\delta^{18}O$ had mostly reached values from –14‰ to –10‰ (C_{18O} = 1975–1984 mg/L) in the uppermost bedrock layer of the ice-free area of the EAB. It means that the infiltration of modern meteoric water M had begun there (Fig. 8B, C). The modern meteoric water filled at least 30% of the total effective porosity of the mixing zone GM in the terrestrial area of the EAB. The contour of $\delta^{18}O = -6‰$ (C_{18O} = 1992 mg/L) in the CVAS had advanced up to 50 km towards the southern and southeastern borders of the EAB with the maximum advancing velocity of about 12 m/year, or 0.03 m/day (Fig. 8D). About 50 km^3 of deep basinal brine had been preserved near the southern border of the EAB at 13.7 ka BP.

Evolution of the Baltic Sea in the Holocene (Models 5, 6 and 7)

The continental ice completely perished from the area of the EAB at the end of the Pleistocene (Kalm et al. 2011). During the period from 12.0 to 10.3 ka BP, the Baltic Ice Lake filled the depressions of the Baltic Sea and the Gulf of Finland flooding the western lowlands of present-day Estonia (Bodén et al. 1997). Between 4.0 and 2.0 ka BP, the Baltic Sea retreated completely from West Estonia and the West Estonian Archipelago. After that, the topography of the EAB remained practically unchanged from the viewpoint of the present study.

The distribution of hydraulic heads completely transformed due to the vanishing of the ice load from the EAB (Figs 9A, 10). Therefore, the encroachment of glacial meltwater into the layers of the EAB ended. The groundwater flow to the southwest ceased in the CVAS

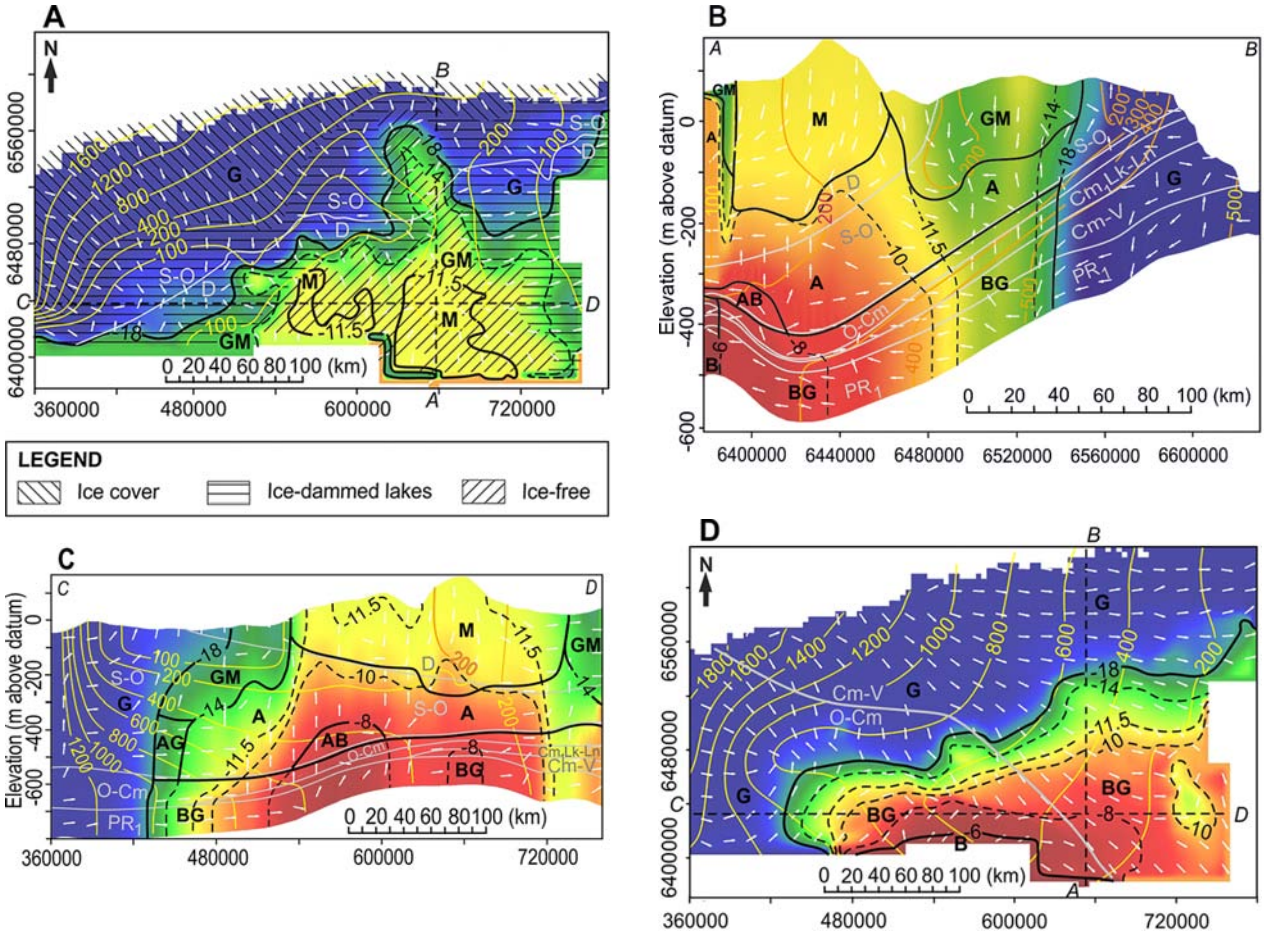

Fig. 8. Groundwater head, flow direction and ^{18}O concentration at 13.7 ka BP (Model 4): (**A**) in the uppermost layers of the bedrock, (**B**) in cross section *A*–*B*, (**C**) in cross section *C*–*D* and (**D**) in the Ordovician–Cambrian and Cambrian–Vendian aquifer systems (see Fig. 7A for legend).

and the groundwater began to flow in the opposite direction under hydraulic head gradients ranging from 0.0002 to 0.0005. The infiltration of modern meteoric water increased twofold, compared to the end of the deglaciation period. In conformity with water budget calculations carried out by means of the HME, the total net infiltration into the Quaternary cover of the EAB was about 6 800 000 m^3/day at 0.1 ka BP (Vallner & Porman 2016). The downward flow from the Quaternary deposits into the underlying bedrock averaged 4 900 000 m^3/day, while the total groundwater discharge in the channel network, big lakes and sea reached 6 300 000 m^3/day. Of the water intruding into the bedrock, the CVAS received approximately 20 000 m^3/day or 0.4%.

The sequential ^{18}O transport simulations by Models 5, 6 and 7 (Table 2) endorsed the results of hydrodynamic calculations, proving that in consequence of the intrusion of modern meteoric water after the deglaciation of the EAB, the ^{18}O mass concentration substantially increased in the groundwater overlying the O–Cm aquifer system (Fig. 9A–C). On the other hand, the general distribution of the simulated ^{18}O concentrations essentially did not change in the CVAS during the Holocene compared to the end of the Pleistocene (Figs 8D, 10). It demonstrated that the velocity of the intruding modern meteoric water into the deep layers of the EAB was relatively low. Therefore, a significant portion of glacial meltwater that accumulated in the CVAS during the Pleistocene and mixed with other genetic types of water has been preserved there to this day.

During the Holocene, the ^{18}O concentration in groundwater underlying the Lükati–Lontova aquitard (Cm_1Lk–Ln) increased markedly due to vertical intrusion of modern meteoric water in the northeastern part of the EAB only (Fig. 10).

The period of intensive groundwater development (Model 8)

Around 1910, a notable withdrawal of deep groundwater by means of bored wells tapping the CVAS began in

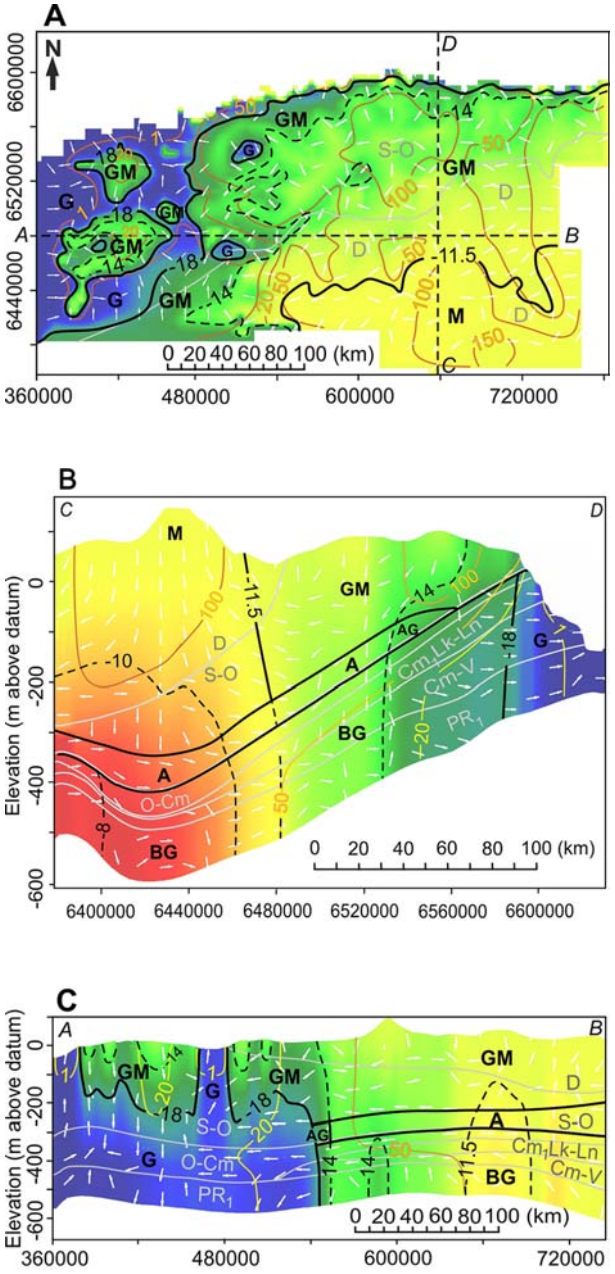

Fig. 9. Groundwater head, flow direction and ^{18}O concentration at 2.0 ka BP (Model 7): (**A**) in the uppermost layers of the bedrock, (**B**) in cross section *C–D* and (**C**) in cross section *A–B* (see Fig. 7A for legend).

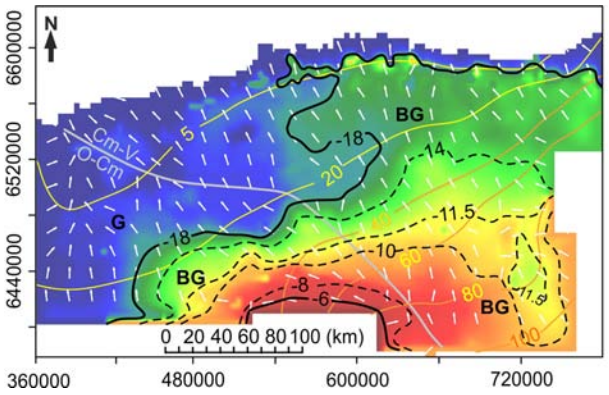

Fig. 10. Groundwater head, flow direction and ^{18}O concentration in the Ordovician–Cambrian aquifer system at 0.1 ka BP, simulated by Model 7 (see Fig. 7A for legend).

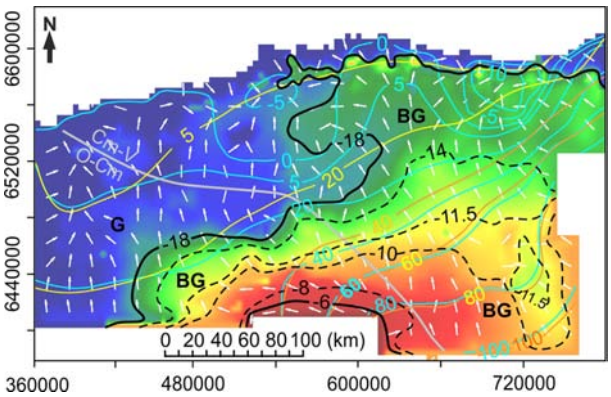

Fig. 11. Groundwater head, flow direction and ^{18}O concentration in the Ordovician–Cambrian and Cambrian–Vendian aquifer systems, simulated by Model 8 (absolute elevation of the groundwater hydraulic head in 1910 and 2016 is shown by *yellow* and *light blue* contours, respectively; see Fig. 7A for other graphical symbols).

Tallinn (Fig. 3) (Perens & Vallner 1997; Vallner & Porman 2016). Later, the total groundwater abstraction grew from about 30 000 m^3/day in 1950 to 470 000 m^3/day in 1991. The basin-wide hydraulic head depressions emerged because of intensive groundwater abstraction (Figs 4, 11). After 1991, the groundwater abstraction for public and industrial supply decreased to 120 000 m^3/day.

The impact of groundwater abstraction on the spatial distribution of hydraulic heads in the EAB was reproduced by Model 8. The pumping rates of groundwater intakes were embedded into this model by means of the VMC boundary condition *Pumping Wells*. Intensive groundwater pumping generated basin-wide and local depressions of hydraulic heads causing cardinal changes in the direction and velocity of filtration flows (Fig. 10). Some of the induced flows promoted the transport of connate brackish water from the deeper portion of the CVAS or seawater intrusion towards groundwater intakes (Marandi & Vallner 2010; Vallner & Porman 2016).

The general distribution of the ^{18}O content recorded for 0.1 ka BP in the EAB changed because of intensive pumping during the groundwater development period. In the vicinity of deep ancient valleys, where the water of upper layers enriched in ^{18}O had intruded into the CVAS, the simulated $\delta^{18}O$ value increased up to 2‰. The greatest changes in $\delta^{18}O$ values occurred in the localities where the transversal permeability of aquitards was relatively high. The ^{18}O transport simulation proved that the CVAS was generally sufficiently isolated from surficial sources of unpotable water. Therefore, the CVAS water must be considered as a strategic resource for emergency situations.

DISCUSSION AND VERIFICATION OF MODELS

The above groundwater flow simulations reconstructed a very complicated geohydrological history from 22 ka BP until the present encompassing drastic changes in hydrodynamic conditions over the entire EAB. The authenticity of the completed calculations was partially assured by the credibility of hydraulic parameters of flow models based on the calibration results of the HME. The adequacy of initial and boundary conditions of the flow models used was more disputable since these were established proceeding from the thickness of the continental ice sheet estimated according to indirect geological evidence.

The most problematic simplification of transport modelling was the presumption that the upper part of the EAB overlying the O–Cm aquifer system was filled with ancient groundwater and lower layers contained basinal brine, whose $\delta^{18}O$ values at 22 ka BP were –14‰ and –6‰, respectively. The postulate was surely a serious distortion of the real situation, but there was no plausible information other than the referenced sources to establish more authentic initial conditions. There was a similar shortage of credible data when stating the ^{18}O concentration for modern meteoric water in the range from –11.5‰ to –8‰.

Thereat it is informative to notice that Sterckx et al. (2018) assigned to their 2D $\delta^{18}O$ models crossing the EAB as two vertical sections (see Fig. 5) the initial $\delta^{18}O$ values equal to –4‰ and –14‰. The $\delta^{18}O$ value of precipitation was equalized to –11‰ during the entire computation period.

The loading efficiency of the continental ice sheet on the hydrodynamics of the subglacial environment was not determined in the current study since reckoning with this phenomenon remained in the interval of other possible miscalculations. Such a conclusion was drawn from an investigation by Lemieux et al. (2008) who simulated subglacial filtration over the entire North American landscape during the Wisconsinian glaciation (from 85 to 11 ka BP). They determined that neglecting the ice load changed the total budget of the subglacial water flows by no more than 5%. For the same reason, the mechanical impact of the glacial load was not taken into account at the modelling of the $\delta^{18}O$ distribution in the EAB carried out by Sterckx et al. (2018).

Because of the previously mentioned allowances and simplifications, the authenticity of simulated $\delta^{18}O$ distribution needs adequate verification. The principal idea of such verification is as follows: *if the flow and transport models completed are correct enough, the simulated concentrations* $C_{18O}(x, y, z, t)$ *by the final Model 8 for the present shall satisfactorily conform to the measured* ^{18}O *concentrations in* C_{18O} *observation points randomly placed over the entire EAB.*

The validity of that criterion was tested by several calibration series of transport models performed by means of VMC (WH 2015). Thereat, mostly the boundary conditions of flow models coupled with transport models were gradually adjusted. The corrections made were local and modest, not exceeding the limits of the geological eventuality.

The adequacy of Model 8 was evaluated by analysing the statistical relationship between simulated and measured ^{18}O absolute concentrations in their 199 observation points (Figs 5, 12; also the Appendix at https://doi.org/10.15152/GEO.501). Also, the statistical relationship between the measured $\delta^{18}O$ values and $\delta^{18}O$ assessments calculated by Eq. (4) for every observation point proceeding from the simulated values of C_{18O} was studied. Among other things, the absolute deviation of measured and calculated $\delta^{18}O$ values was estimated (column $\left|\ \text{‰}\ \right|$ in the online Appendix). The correlation coefficient between measured and simulated ^{18}O absolute concentrations was 0.862 and the same between measured and calculated $\delta^{18}O$ values was 0.863.

The other results of the statistical investigation are given in Table 4.

A supplementary test was carried out to appraise the impact of the postulated initial and boundary conditions on the results of transport modelling. Specific observation points of five main bedrock aquifers were selected for the study of the ^{18}O concentration history in the EAB. Points 9, 21, 66, 91 and 175 expressed the best fit of simulated and measured ^{18}O concentrations obtained by Model 8. The maximum positive deviations of simulated values from measured ones were recorded in points 11, 63, 97 and 177, maximum negative deviations in points 13, 17, 42, 71 and 169. The locations of these observation points were virtually embedded into all complementary models preceding Model 8.

The ^{18}O concentrations simulated in virtual observation points for the period from 22 ka BP until 2016 are given in Fig. 13A, B. According to the graphs, the ^{18}O concentration was diluted in all the virtual observation points because of the intensive encroachment of glacial water into the layers of the EAB from 22 until 18 ka BP.

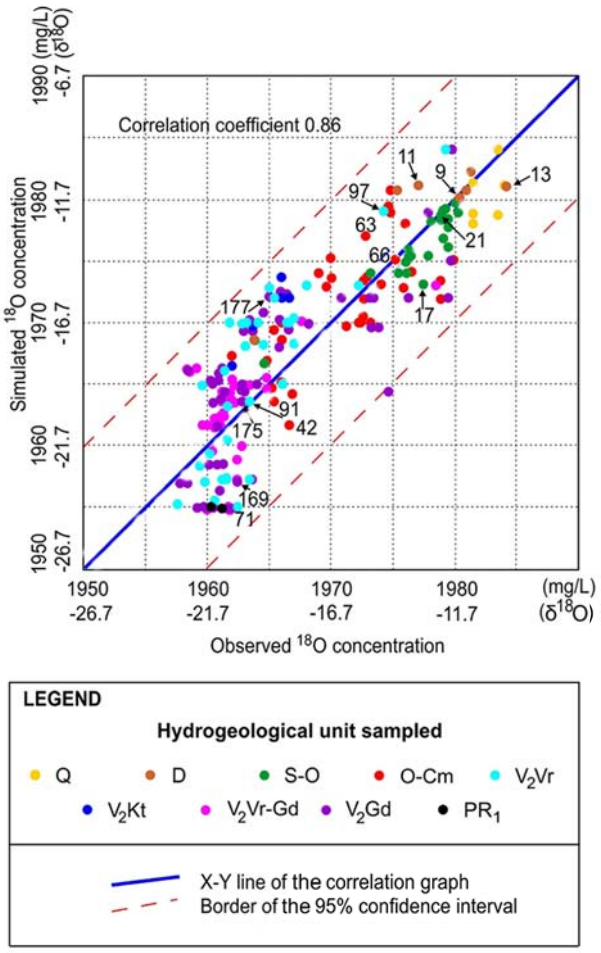

Fig. 12. Calibration graph of Model 8. The numbered points are used in the text at the consideration of the ^{18}O concentration history (see Fig. 5 for the affiliation of points to hydrogeological units and the Appendix at https://doi.org/10.15152/GEO.501 for detailed data). A 95% confidence interval visualizes the range of calculated values for each observed value with 95% confidence that the simulation results are acceptable for the given observed value (WH 2015).

The diluted ^{18}O concentrations were preserved in the Ordovician–Cambrian and Cambrian–Vendian aquifer systems until 12 ka BP, but afterwards, the concentrations began to rise again due to the recovered intrusion of meteoric water (Fig. 13A). However, the influence of meteoric water was relatively weak in some deeper parts of the bedrock isolated from the ground surface by more effective aquitards (points 42, 71, 91, 169 and 175). The increase in ^{18}O concentrations in the Devonian and Silurian–Ordovician aquifer systems after the glaciation varied more due to diverse infiltration conditions in the upper layers (Fig. 13B).

In spite of all the radical changes in the calculated ^{18}O concentrations in the last 22 ka, their final values converged quite close to the measured values of ^{18}O in the set of the existing observation points (Fig. 5). This demonstrates additionally that the time-dependent spatial development of simulated ^{18}O concentrations was in logical and quantitative accordance with the hydrodynamic situation established by flow models. In principle, it was even possible to diminish the discrepancy between the measured and simulated ^{18}O mass concentrations using the contemporary methods of inverse modelling. However, it was not essential for the present study.

Thus, the statistical assessment of the discrepancies between the simulated ^{18}O concentrations and their measured values, as well as the analysis of the ^{18}O concentration history in virtual observation points, verify the sufficient adequacy of the above groundwater flow calculations performed for the EAB for the period from 22 ka BP until the present. The time-dependent spatial distribution of ^{18}O concentrations simulated for the entire EAB and statistically accredited by the data from 199 observation points could at least be considered as a sufficiently founded scientific hypothesis. It confirms the results of hydrodynamic simulations explaining the impact of glaciation, its regression and the intensive groundwater abstraction on the EAB's water regime.

Table 4. Statistical characteristics of measured and simulated ^{18}O values

Statistical characteristic	Absolute ^{18}O concentration (mg/L)			Relative ^{18}O concentration (‰)		
	Measured	Simulated	Residual	Measured	Calculated	Residual (absolute value)
Minimum value	1957.6	1955.0	–10.2	–22.9	–24.2	0.0
Maximum value	1984.1	1984.0	8.2	–9.7	–9.7	5.1
Absolute residual mean	3.445			1.732		
Standard error of the estimate	0.296			0.079		
Root mean squared (RMS)	4.11			2.06		

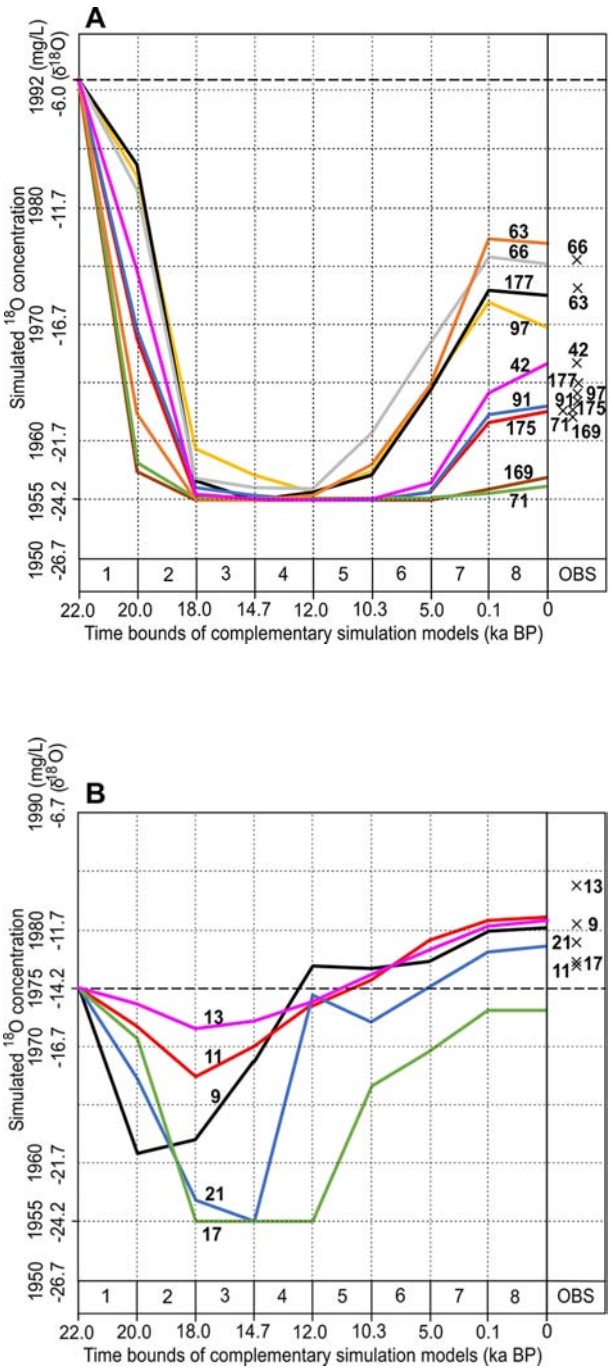

Fig. 13. The ^{18}O concentration simulated in virtual observation points during the entire modelling period: (**A**) the Ordovician–Cambrian and Cambrian–Vendian aquifer systems, (**B**) the Devonian and Silurian–Ordovician aquifer systems (see Fig. 5 for the affiliation of points to hydrogeological units and the Appendix at https://doi.org/10.15152/GEO.501). *Dashed lines* show the initial ^{18}O concentration at 22 ka BP. *Skew crosses* mark the measured ^{18}O concentrations in observation points (column OBS).

SUMMARY AND CONCLUSIONS

This paper describes how to perform a coupled simulation of the groundwater flow and ^{18}O concentration in a basin-wide aquifer system to verify the results of regional hydrodynamic calculations. The hydrogeologically profoundly studied Estonian Artesian Basin (EAB) was selected as a study area to check the applicability of the proposed method in real-world conditions. The distribution of the hydraulic head and ^{18}O concentration as a continuous function $C_{18O}(x, y, z, t)$ were simulated by eight sequential mutually connected transport models together forming an integrated calculation unit. The adequacy of flow and transport modellings completed for the last 22 ka was verified by a statistically acceptable correspondence between the observed and simulated final values of the ^{18}O concentration in 199 observation points randomly situated over the entire EAB.

According to hydrodynamic simulations, the former discharge of basinal brine and ancient groundwater from the layers of the EAB into the depressions of the Baltic Sea and the Gulf of Finland ceased at the beginning of the last glaciation in the Late Pleistocene. The glacial meltwater encroached transversally into the uppermost layers and laterally into deeper ones. Deep groundwater, including basinal brines, moved upwards, being drained by a network of subglacial currents. By the end of the glaciation, the maximum extent of glacial meltwater in deep layers almost reached the southern border of the EAB. During the deglaciation and evolution of the Baltic Sea, modern meteoric water intruded into the upper layers filled earlier with glacial meltwater. Once again, deep groundwater began to move towards the Baltic Sea and the Gulf of Finland. Ancient groundwater, basinal brine, glacial meltwater and modern meteoric water intermingled in various proportions due to drastic changes in the hydrodynamic situation.

The study additionally proved the adequacy of the EAB's hydraulic parameters used for simulations, explained the history of groundwater formation and clarified the isolation capability of the aquitards. This helps elaborate on the optimum management of water resources.

The main results of the paper are as follows:

- It has been proved that a three-dimensional time-dependent distribution of ^{18}O concentration as a boundary problem of groundwater transport in a regional-scale heterogeneous multi-layered aquifer system can be numerically simulated by codes MODFLOW-2005 and MT3DMS.
- An optimum method of the transition of the observed negative $\delta^{18}O$ values to respective positive units of the absolute ^{18}O concentration needed for simulations has been substantiated and practically implemented.

- The history of groundwater formation in the EAB during the Late Pleistocene and Holocene has been reconstructed and interpreted, based on hydrodynamic calculations proved by the distribution of the simulated ^{18}O concentrations.
- The completed set of groundwater flow and ^{18}O transport models functionally connected is an acceptable integral hydrogeological model of the Estonian Artesian Basin for the time span from 22 ka BP until the present. The Geological Survey of Estonia used it in 2019–2020 to elaborate the scientifically grounded principles of the optimum development of the Estonian water environment.
- The current study contributes to a wider application of ^{18}O data in the investigation of the complicated problem of groundwater flow and transport in real-world conditions. This is a scientific innovation for tracer application in hydrogeological methodology.

Acknowledgements. The activities of the present study were supported by Estonian Science Foundation Grant ETF8948. The paper is a contribution to Estonian Research Council Project IUT19-22, IAEA CRP:F33019 (Contract No. 17850) and INQUA/UNESCO supported G@GPS Project. We are grateful to the anonymous referees for constructive reviews of the paper. We thank Tõnu Martma for $\delta^{18}O$ analysis, Helle Pohl-Raidla for improvement of the English and Joonas Pärn for helpful comments. Through the years, many people have contributed to the compilation of the isotope-geochemical database of groundwater of the Department of Geology, Tallinn University of Technology, used as the main data source for this paper. The authors would like to thank all the contributors. The publication costs of this article were partially covered by the Estonian Academy of Sciences.

Supplementary online data

Supplementary material can be found in the Appendix at https://doi.org/10.15152/GEO.501. The Appendix contains general characteristics of sampling points shown in Fig. 5 together with measured and simulated ^{18}O data.

REFERENCES

Arppe, L. & Karhu, J. A. 2010. Oxygen isotope values of precipitation and the thermal climate in Europe during the middle to late Weichselian ice age. *Quaternary Science Reviews*, **29**, 1263–1275.

Babre, A., Kalvāns, A., Popovs, K., Retiķe, I., Dēliņa, A., Vaikmäe, R. & Martma, T. 2016. Pleistocene age paleo-groundwater inferred from water-stable isotope values in the central part of the Baltic Artesian Basin. *Isotopes in Environmental and Health Studies*, **52**, 706–725.

Beal, L. K., Wong, C. I., Bautista, K. K., Jenson, J. W., Banner, J. L., Lander, M. A., Gingerich, S. B., Partin, J. W., Hardt, B. & van Oort, N. H. 2019. Isotopic and geochemical assessment of the sensitivity of groundwater resources of Guam, Mariana Islands, to intra- and inter-annual variations in hydroclimate. *Journal of Hydrology*, **568**, 174–183.

Bear, J. & Cheng, A. H.-D. 2010. *Modeling Groundwater Flow and Contaminant Transport*. Springer, Dordrecht, Heidelberg, London, New York, 834 pp.

Beaudoin, G., Therrien, R. & Savard, C. 2006. 3D numerical modelling of fluid flow in the Val-d'Or orogenetic gold district: major crustal shear zones drain fluids from overpressured vein fields. *Mineralium Deposita*, **41**, 82–98.

Bense, V. F. & Person, M. A. 2008. Transient hydrodynamics within intercratonic sedimentary basins during glacial cycles. *Journal of Geophysical Research*, **113**, F04005, 17 pp.

Bodén, P., Fairbanks, R. G., Wright, J. D. & Burckle, L. H. 1997. High-resolution stable isotope records from southwest Sweden: the drainage of the Baltic Ice Lake and Younger Dryas ice margin oscillations. *Paleoceanography*, **12**, 39–49.

Boulton, G. S., Caban, P. E. & Van Gijssel, K. 1995. Groundwater flow beneath ice sheets: part 1 – large scale patterns. *Quaternary Science Reviews*, **14**, 545–562.

Bowman, J. R. & Willett, S. D. 1991. Spatial patterns of oxygen isotope exchange during one-dimensional fluid infiltration. *Geophysical Research Letters*, **18**, 971–974.

Clark, I. D. & Fritz, P. 1997. *Environmental Isotopes in Hydrogeology*, first ed. CRC Press/Lewis Publishers, Boca Raton, 352 pp.

Coplen, T. B., Hopple, J. A., Böhlke, J. K., Peiser, H. S., Rieder, S. E., Krouse, H. R., Rosman, K. J. R., Ding, T., Vocke, R. D. Jr., Révész, K. M., Lamberty, A., Taylor, P. & De Bièvre, P. 2002. *Compilation of Minimum and Maximum Isotope Ratios of Selected Elements in Naturally Occurring Terrestrial Materials and Reagents*. U.S. Geological Survey, Water-Resources Investigations Report 01-4222, Reston, 98 pp.

Crank, J. 1975. *The Mathematics of Diffusion*, second ed. Clarendon Press, Oxford, 424 pp.

DeFoor, W., Person, M., Larsen, H. C., Lizarralde, D., Cohen, D. & Dugan, B. 2011. Ice sheet-derived submarine groundwater discharge on Greenland's continental shelf. *Water Resources Research*, **47**, W07549.

Diersch, H.-J. G. 2014. *FEFLOW*. Springer, Berlin, Heidelberg, 996 pp.

Elverhøi, A., Fieldskaar, W., Solheim, A., Nyland-Berg, M. & Russwurm, L. 1993. The Barents Sea ice sheet – a model of its growth and decay during the last ice maximum. *Quaternary Science Reviews*, **12**, 863–873.

Fetter, C. W. 1993. *Contaminant Hydrogeology*. Macmillan Publishing Company, New York, 458 pp.

Gavrilova, O., Vilu, R. & Vallner, L. 2010. A life cycle environmental impact assessment of oil shale produced and consumed in Estonia. *Resources, Conservation and Recycling*, **55**, 232–245.

GeoRepository. 2016. *Estonian Coordinate System of 1997*. https://georepository.com/crs_3301/Estonian-Coordinate-System-of-1997.html [accessed 27 January 2020].

Gerber, C., Vaikmäe, R., Aeschbach, W., Babre, A., Jiang, W., Leuenberger, M., Lu, Z.-T., Mokrik, R., Müller, P., Raidla, V., Saks, T., Waber, H. N., Weissbach, T., Zappala, J. C. & Purtschert, R. 2017. Using 81Kr and noble

gases to characterize and date groundwater and brines in the Baltic Artesian Basin on the one-million-year timescale. *Geochimica et Cosmochimica Acta*, **205**, 187–210.

Gonçalvès, J., Vallet-Coulomb, C., Petersen, J., Hamelin, B. & Deschamps, P. 2015. Declining water budget in a deep regional aquifer assessed by geostatistical simulations of stable isotopes: Case study of the Saharan ''Continental Intercalaire". *Journal of Hydrology*, **531**, 821–829.

Grathwohl, P. 1998. *Diffusion in Natural Porous Media: Contaminant Transport, Sorption/Desorption, and Dissolution Kinetics*. Kluwer Academic Publishers, Boston, 207 pp.

Harbaugh, A. W. 2005. *MODFLOW-2005, the U.S. Geological Survey Modular Ground-Water Model – the Ground-Water Flow Process*. USGS Techniques and Methods 6-A16, Reston, 253 pp.

Huysmans, M. & Dassargues, A. 2005. Review of the use of Péclet numbers to determine the relative importance of advection and diffusion in low permeability environments. *Hydrogeology Journal*, **13,** 895–904.

IAEA. 2017. *Reference Sheet for International Measurement Standards. VSMOW2 & SLAP2 Reference Sheet*. International Atomic Energy Agency (IAEA), Vienna, 8 pp.

IAEA/WMO. 2018. WISER-Water Isotope System for data analysis, visualization and Electronic Retrieval. https://nucleus.iaea.org/wiser/index.aspx [accessed 30 April 2020].

Jiang, Z., Xua, T., Mallants, D., Tiana, H. & Owen, D. D. R. 2019. Numerical modelling of stable isotope (^{2}H and ^{18}O) transport in a hydrogeothermal system: Model development and implementation to the Guide Basin, China. *Journal of Hydrology*, **569**, 93–105.

Jiráková, H., Huneau, F., Celle-Jeanton, H., Hrkal, Z. & Le Coustumer, P. 2011. Insights into palaeorecharge conditions for European deep aquifers. *Hydrogeology Journal*, **19**, 1545–1562.

Kalm, V., Raukas, A., Rattas, M. & Lasberg, K. 2011. Pleistocene glaciations in Estonia. *Developments in Quaternary Sciences*, **15**, 95–104.

Kern, Z., Kohán, B. & Leunberger, M. 2014. Precipitation isoscape of high reliefs: interpolation scheme designed and tested for monthly resolved precipitation oxygen isotope records of an Alpine domain. *Atmospheric Chemistry and Physics*, **14**, 1897–1907.

Koit, O., Barberác, J. A., Marandi, A., Terasmaaa, J., Kiivita, I.-K. & Martma, T. 2020. Spatiotemporal assessment of humic substance-rich stream and shallow karst aquifer interactions in a boreal catchment of northern Estonia. *Journal of Hydrology*, **580**, 124–238.

Kortelainen, N. 2007. *Isotopic Fingerprints in Surficial Waters: Stable Isotope Methods Applied in Hydrogeological Studies*. Geological Survey of Finland, Espoo, 39 pp.

Kumar, M., Ramanathan, A., Mukherjee, A., Sawlani, R. & Ranjan, S. 2019. Delineating sources of groundwater recharge and carbon in Holocene aquifers of the central Gangetic basin using stable isotopic signatures. *Isotopes in Environmental and Health Studies*, **55**, 254–271.

Lambeck, K., Purcell, A., Zhao, J. & Svensson, N. O. 2009. The Scandinavian ice sheet: from MIS 4 to the end of the Last Glacial Maximum. *Boreas*, **39**, 410–443.

Lasberg, K. & Kalm, V. 2013. Chronology of Late Weichselian glaciation in the western part of the East European Plain. *Boreas*, **42**, 995–1007.

Lemieux, J. M., Sudicky, E., Peltier, W. & Tarasov, L. 2008. Dynamics of groundwater recharge and seepage over the Canadian landscape during the Wisconsinian glaciation. *Journal of Geophysical Research*, **113**, F01011, 18 pp.

Li, Z., Yang, Q., Yang, Y., Ma, H., Wang, H., Luoa, J., Bian, J. & Martin, J. D. 2019. Isotopic and geochemical interpretation of groundwater under the influences of anthropogenic activities. *Journal of Hydrology*, **576**, 685–697.

Liedl, R., Yadav, P. K. & Dietrich, P. 2011. Length of 3-D mixing-controlled plumes for a fully penetrating contaminant source with finite width. *Water Resources Research*, **47**, W08602.

Malov, A. I. & Tokarev, I. V. 2019. Using stable isotopes to characterize the conditions of groundwater formation on the eastern slope of the Baltic Shield (NW Russia). *Journal of Hydrology*, **578**, 124–130.

Marandi, A. & Vallner, L. 2010. Upconing of saline water from the crystalline basement into the Cambrian–Vendian aquifer system on the Kopli Peninsula, northern Estonia. *Estonian Journal of Earth Sciences*, **59**, 277–287.

Marandi, A., Osjamets, M., Polikarpus, M., Pärn, J., Raidla, V., Tarros, S. & Vallner, L. 2019. *Põhjaveekogumite piiride kirjeldamine, koormusallikate hindamine ja hüdrogeoloogiliste kontseptuaalsete mudelite koostamine* [*Delineation of Groundwater Bodies in Estonia, Assessment of Their Stress Sources and Completing Conceptual Models*]. Eesti Geoloogiateenistus, Rakvere, 536 pp. [in Estonian].

McIntosh, J. C., Schlegel, M. E. & Person, M. 2012. Glacial impacts on hydrologic processes in sedimentary basins: evidence from natural tracer studies. *Geofluids*, **12**, 7–21.

McKinney, C. R., McCrea, J. M., Epstein, S., Allen, H. A. & Urey, H. C. 1950. Improvements in mass spectrometers for the measurement of small differences in isotope abundance ratios. *Review of Scientific Instruments*, **21**, 724–730.

Mokrik, R. 2003. *The Palaeohydrogeology of the Baltic Basin. Neoproterozoic & Phanerozoic*. Vilnius University Publishing House, Vilnius, 135 pp.

Mokrik, R. & Mažeika, J. 2002. Paleohydrogeological reconstruction of groundwater recharge during Late Weichselian in the Baltic Basin. *Geologija (Vilnius)*, **39**, 49–57.

Ogata, A. & Banks, R. B. 1961. *A Solution of the Differential Equation of Longitudinal Dispersion in Porous Media*. U.S. Geological Survey Professional Paper 411-A, Washington, 12 pp.

Olausson, E. 1982. Stable isotopes. In *The Pleistocene/Holocene Boundary in South-Western Sweden* (Olausson, E., ed.), *Sveriges Geologiska Undersökning, Serie C*, **794**, 82–92.

Pärn, J., Vaikmäe, R., Raidla, V., Martma, T., Ivask, J., Kaup, E., Vallner, L., Putschert, R., Gerber, C., Aeschbach-Hertig, W. & Weissbach, T. 2015. Overview of groundwater studies in the Baltic Artesian Basin at Tallinn University of Technology. In *4th Annual Meeting of G@GPS. IGCP 618 Project. Paleogroundwater from Past and Present Glaciated Areas. Estonia, 5–9 July 2015* (Pärn, J., Raidla, V., Vaikmäe, R., Raukas, A. & Bauert, H., eds), pp. 21–23. Tallinn University of Technology, Tallinn.

Pärn, J., Raidla, V., Vaikmäe, R., Martma, T., Ivask, J., Mokrik, R. & Erg, K. 2016. The recharge of glacial meltwater and its influence on the geochemical evolution of groundwater in the Ordovician-Cambrian aquifer system, northern part of the Baltic Artesian Basin. *Applied Geochemistry*, **72**, 125–135.

Pärn, J., Walraevens, K., van Camp, M., Raidla, V., Aeschbach, W., Friedrich, R., Ivask, J., Kaup, E., Martma, T., Mažeika, J., Mokrik, R., Weissbach, T. & Vaikmäe, R. 2019. Dating of glacial palaeogroundwater in the Ordovician-Cambrian aquifer system, northern Baltic Artesian Basin. *Applied Geochemistry*, **102**, 64–76.

Perens, R. & Vallner, L. 1997. Water-bearing formation. In *Geology and Mineral Resources of Estonia* (Raukas, A. & Teedumäe, A., eds), pp. 137–145. Estonian Academy Publishers, Tallinn.

Person, M., Bense, V., Cohen, D. & Banerjee, A. 2012a. Models of ice-sheet hydrogeologic interactions: a review. *Geofluids*, **12**, 58–78.

Person, M., Marksamer, A., Dugan, B., Sauer, P. E., Brown, K., Bish, D., Licht, K. J. & Willett, M. 2012b. Use of a vertical $\delta^{18}O$ profile to constrain hydraulic properties and recharge rates across a glacio-lacustrine unit, Nantucket Island, Massachusetts, USA. *Hydrogeology Journal*, **20**, 325–336.

Punning, J.-M., Toots, M. & Vaikmäe, R. 1987. Oxygen-18 in Estonian natural waters. *Isotopenpraxis*, **23**, 232–234.

Raidla, V., Kirsimäe, K., Vaikmäe, R., Jõeleht, A., Karro, E., Marandi, A. & Savitskaja, L. 2009. Geochemical evolution of groundwater in the Cambrian–Vendian aquifer system of the Baltic Basin. *Chemical Geology*, **258**, 219–231.

Raidla, V., Kirsimäe, K., Vaikmäe, R., Kaup, E. & Martma, T. 2012. Carbon isotope systematics of the Cambrian–Vendian aquifer system in the northern Baltic Basin: implications to the age and evolution of groundwater. *Applied Geochemistry*, **27**, 2042–2052.

Raidla, V., Kern, Z., Pärn, J., Babre, A., Erg, K., Ivask, J., Kalva, A., Kohán, B., Lelgus, M., Martma, T., Mokrik, R., Popovs, K. & Vaikmäe, R. 2016. A $\delta^{18}O$ isoscape for the shallow groundwater in the Baltic Artesian Basin. *Journal of Hydrology*, **542**, 254–267.

Raidla, V., Pärn, J., Schloemer, S., Aeschbach, W., Czuppon, G., Ivask, J., Marandi, A., Sepp, H., Vaikmäe, R. & Kirsimäe, K. 2019. Origin and formation of methane in groundwater of glacial origin from the Cambrian-Vendian aquifer system in Estonia. *Geochimica et Cosmochimica Acta*, **251**, 247–264.

Raukas, A. 1986. Deglaciation of the Gulf of Finland and adjoining areas. *Bulletin of the Geological Society of Finland*, **58**, 21–33.

Shackleton, C., Patton, H., Hubbard, A., Winsborrow, M., Kingslake, J., Esteves, M., Andreassen, K., Sarah, L. & Greenwood, S. L. 2018. Subglacial water storage and drainage beneath the Fennoscandian and Barents Sea ice sheets. *Quaternary Science Reviews*, **201**, 13–28.

Siegert, M. J. 2001. *Ice Sheets and Late Quaternary Environmental Change*. John Wiley & Sons LTD, Chichester, 231 pp.

Sofer, Z. & Gat, J. R. 1972. Activities and concentrations of oxygen-18 in concentrated aqueous salt solutions: analytical and geophysical implications. *Earth and Planetary Science Letters*, **15**, 232–238.

Sterckx, A., Lemieux, J.-M. & Vaikmäe, R. 2018. Assessment of paleo-recharge under the Fennoscandian Ice Sheet and its impact on regional groundwater flow in the northern Baltic Artesian Basin using a numerical model. *Hydrogeology Journal*, **26**, 2793–2810.

Stotler, R. L., Frape, S. K., Ruskeeniemi, T., Pitkänen, P. & Blowes, D. W. 2012. The interglacial–glacial cycle and geochemical evolution of Canadian and Fennoscandian Shield groundwaters. *Geochimica et Cosmochimica Acta*, **76**, 45–67.

Therrien, R., McLaren, R. G., Sudicky, E. A. & Park, Y.-J. 2012. *HydroGeoSphere. A Three-Dimensional Numerical Model Describing Fully-Integrated Subsurface and Surface Flow and Solute Transport*. Groundwater Simulations Group, Waterloo, 456 pp.

Vaikmäe, R. & Vallner, L. 1990. Oxygen-18 in Estonian groundwaters. In *Fifth Working Meeting: Isotopes in Nature, Leipzig, 25–29 September 1989* (Wand, U. & Strauch, G., eds), pp. 161–162. Central Institute of Isotope and Radiation Research Leipzig, Leipzig.

Vaikmäe, R., Vallner, L., Loosli, H. H., Blaser, P. C. & Julliard-Tardent, M. 2001. Paleogroundwater of glacial origin in the Cambrian-Vendian aquifer of northern Estonia. In *Paleowaters in Coastal Europe: Evolution of Groundwater since the Late Pleistocene* (Edmunds, W. M. & Milne, C. J., eds), *Geological Society London, Special Publications*, **189**, 17–27.

Vaikmäe, R., Kaup, E., Marandi, A., Martma, T., Raidla, V. & Vallner, L. 2008. The Cambrian-Vendian aquifer, Estonia. In *The Natural Baseline Quality of Groundwater* (Edmunds, W. M. & Shand, P., eds), pp. 175–189. Blackwell Publishing, Oxford.

Vaikmäe, R., Martma, T., Ivask, J., Kaup, E., Raidla, V., Rajamäe, R., Vallner, L., Mokrik, R., Samalavičius, V., Kalvāns, A., Babre, A., Marandi, A., Hints, O. & Pärn, J. 2020. Baltic groundwater isotope-geochemistry database. Department of Geology, Tallinn University of Technology. https://doi.org/10.15152/GEO.488 [accessed 10 June 2020].

Vallner, L. 2003. Hydrogeological model of Estonia and its applications. *Proceedings of the Estonian Academy of Sciences, Geology*, **52,** 179–192.

Vallner, L. & Porman, A. 2016. Groundwater flow and transport model of the Estonian Artesian Basin and its hydrological developments. *Hydrology Research*, **47**, 814–834.

Vallner, L., Gavrilova, O. & Vilu, R. 2015. Environmental risks and problems of the optimal management of an oil shale semi-coke and ash landfill in Kohtla-Järve, Estonia. *Science of the Total Environment*, **524**–**525**, 400–415.

van Genuchten, M. T. & Alves, W. J. 1982. *Analytical Solutions of the One-Dimensional Convective-Dispersive Solute Transport Equation*. U.S. Department of Agriculture, Technical Bulletin No. 1661, 151 pp.

Wassenaar, L. I., Van Wilgenburg, S. L., Larson, K. & Hobson, K. A. 2009. A groundwater isoscape (δD, $\delta^{18}O$) for Mexico. *Journal of Geochemical Exploration*, **102**, 123–136.

WH. 2015. *Visual MODFLOW 2011.1 User's Manual*. Waterloo Hydrogeologic, Inc., Waterloo, 712 pp.

Winston, R. B. 2019. *ModelMuse Version 4 – A Graphical User Interface for MODFLOW 6*: U.S. Geological Survey Scientific Investigations Report 2019–5036, 10 pp.

Yates, S. R. 1992. An analytical solution for one-dimensional transport in porous media with an experimental dispersion function. *Water Resources Research*, **28**, 2149–2154.

Zhao, L. J., Easto, C. J., Liu, X. H., Wang, L. X., Wang, N. L., Xie, C. & Song. Y. X. 2018. Origin and residence time of groundwater based on stable and radioactive isotopes in the Heihe River Basin, northwestern China. *Journal of Hydrology: Regional Studies*, **18**, 31–49.

Zheng, C. 2010. *MT3DMS v5.3: A Modular Three-Dimensional Multispecies Transport Model for Simulation of Advection, Dispersion and Chemical Reactions of Contaminants in Groundwater Systems. Supplemental User's Guide.* The University of Alabama, U.S. Army Corps of Engineers, Vicksburg, 56 pp.

Zheng, C. & Bennett, G. D. 2002. *Applied Contaminant Transport Modeling*, second ed. John Wiley & Sons, New York, 621 pp.

Zheng, C. & Wang, P. P. 1998. *MT3DMS. A Modular Three-Dimensional Multispecies Transport Model for Simulation of Advection, Dispersion and Chemical Reactions of Contaminants in Groundwater Systems. (Release DoD_3.00.A). Documentation and User's Guide*. US Army Corps of Engineers, Vicksburg, 220 pp.

Zheng, C. & Wang, P. P. 1999. *A Modular Three-Dimensional Multispecies Transport Model for Simulation of Advection, Dispersion and Chemical Reactions of Contaminants in Groundwater Systems; Documentation and User's Guide. Final Report*. Department of Geological Sciences, University of Alabama, Tuscaloosa, 203 pp.

Zuber, A., Rozanski, K., Kania, J. & Purtschert, R. 2011. On some methodological problems in the use of environmental tracers to estimate hydrogeologic parameters and to calibrate flow and transport models. *Hydrogeology Journal*, **19**, 53–60.

^{18}O kontsentratsiooni mittestatsionaarne 3D-mudeldamine programmipakettidega MODFLOW-2005 ja MT3DMS regionaalse ulatusega põhjavee-kihtkonnas Eesti arteesiabasseini näitel

Leo Vallner, Jüri Ivask, Andres Marandi, Rein Vaikmäe, Valle Raidla ja Anto Raukas

Tõestati, et matemaatilise füüsika rajaülesandena seatud ^{18}O kontsentratsiooni ajast sõltuv kolmemõõtmeline jaotumus regionaalse ulatusega ja muutliku juhtivusega põhjavee-kihtkonnas on numbriliselt mudeldatav hüdrogeoloogias üldtuntud programmipakettidega MODFLOW-2005 ja MT3DMS. Põhjendati optimaalne viis mõõdetud negatiivsete δ^{18}O väärtuste transformeerimiseks mudeldamise jaoks vajalikeks ^{18}O absoluutse kontsentratsiooni ühikuteks. Väljatöötatud arvutusmetoodika praktilise rakendatavuse tõestamiseks rekonstrueeriti ja interpreteeriti Eesti arteesiabasseini geohüdroloogiline arengulugu Hilis-Pleistotseenis ning Holotseenis. Tehtud regionaalsete hüdrogeoloogiliste arvutuste adekvaatsus tõestati vaadeldud ja arvutatud ^{18}O kontsentratsiooni väärtuste tugeva korrelatiivse seosega. Konstrueeriti Eesti arteesiabasseini põhjavee voolu- ja transpordimudelite integraalne süsteem, mis on rakendatav viimase 22 000 aasta kestel toimunud ning ka tulevaste hüdrogeoloogiliste protsesside uurimiseks. Seda kasutas Eesti Geoloogiateenistus aastatel 2019–2020 Eesti veekeskkonna seisundi optimeerimiskavade põhjendamisel.